

Rochester Institute of Technology

## RIT Digital Institutional Repository

---

### Theses

---

12-7-2006

## Investigation of poly[4(5)-vinylimidazole] composites and their potential as proton conductive membranes

Jinghang Wu

Follow this and additional works at: <https://repository.rit.edu/theses>

---

### Recommended Citation

Wu, Jinghang, "Investigation of poly[4(5)-vinylimidazole] composites and their potential as proton conductive membranes" (2006). Thesis. Rochester Institute of Technology. Accessed from

This Thesis is brought to you for free and open access by the RIT Libraries. For more information, please contact [repository@rit.edu](mailto:repository@rit.edu).

# INVESTIGATION OF POLY[4(5)-VINYLMIDAZOLE] COMPOSITES AND THEIR POTENTIAL AS PROTON CONDUCTIVE MEMBRANES

**JINGHANG WU**

**August 2006**

Thesis submitted in partial fulfillment of the requirements for the degree of  
Master of Science in Materials Science and Engineering

**Approved:** \_\_\_\_\_

Thomas W. Smith (Advisor)

**Accepted:** \_\_\_\_\_

Dr. K.S. V. Santhanam (Director)

**Department of Materials Science and Engineering  
Rochester Institute of Technology  
Rochester, New York 14623-5603**

**Copyright Release Form:**

INVESTIGATION OF POLY[4(5)-VINYLMIDAZOLE] COMPOSITES  
AND THEIR POTENTIAL AS PROTON CONDUCTIVE MEMBRANES

I, Jinghang Wu, hereby grant permission to the Wallace Memorial Library of Rochester Institute of Technology to reproduce my thesis in whole or in part. Any reproduction will not be for commercial use or profit.

---

Jinghang Wu

August 2006

## Table of contents

Table of contents	iii
Abstract	v
Acknowledgement	vii
List of Tables	viii
List of Figures	ix
<b>Introduction and background</b>	<b>1</b>
○ <i>Sulfonic acid ionomer membranes</i>	3
○ <i>Polybenzimidazole/H<sub>3</sub>PO<sub>4</sub> membranes</i>	5
○ <i>Composites with inorganic materials</i>	6
– Sulfonic acid ionomer membrane composites with inorganic materials ranging from oxides to lamellar zirconium phosphates or phosphonates	
– Inert polymers filled with ionomers or inorganic particles possessing high proton conductivity	
○ <i>Imidazole Systems</i>	7
<b>Experimental</b>	<b>11</b>
○ <i>Materials</i>	
○ <i>4(5)-vinylimidazole</i>	
○ <i>Polymerization of 4(5)-vinylimidazole in benzene solution</i>	
○ <i>Polymerization of 4(5)-vinylimidazole in ethanol/water solution</i>	
○ <i>15% Weight % solution of PVdF in DMF</i>	
○ <i>15 Weight % solution of poly[4(5)-vinylimidazole in DMF</i>	
○ <i>PVdF/poly[4(5)-vinylimidazole]/bis-trifluoromethylsulfonylimide composite Films</i>	
○ <i>Crosslinked PVdF/poly[4(5)-vinylimidazole]/bis-trifluoromethylsulfonylimide composite films</i>	
○ <i>Characterization of the composite films</i>	
– Differential Scanning Calorimetry (DSC)	
– Thermal gravimetric analysis (TGA)	
– Polarized, Hot-stage Microscopy	
– Proton Conductivity	
○ <i>NMR</i>	17

<b>Results and discussions</b>	18
A. <i>Fabrication of PVdF/poly[4(5)-vinylimidazole/imidazolium TFSI] composite films</i>	19
B. <i>Characterization of the composite films</i>	23
1. Polarized light microscopy	17
2. Differential Scanning Calorimetry (DSC )	26
3. Thermal Gravimetric Analysis (TGA)	33
C. <i>Proton conductivity</i>	38
<b>Summary and Next Steps</b>	41
<b>References</b>	43

## Abstract

In order to demonstrate proton conductivity in an imidazole polymer system, novel composite proton exchange membranes were fabricated by casting films of poly[4(5)-vinylimidazole/vinylimidazolium trifluoromethylsulfonylimide] and poly(vinylidene fluoride)], PVdF, from mixed dimethylformamide (DMF) solutions. The phase, composition and morphology of these composites were examined by differential scanning calorimetry (DSC), and hot stage polarized microscopy. Thermal stability was evaluated by thermal gravimetric analysis (TGA). Proton conductivity was in a fuel cell test fixture evaluated at GM Fuel Cell Activities in Honeoye Falls, NY.

DSC thermograms were characterized by a crystalline melt for the PVdF component at  $\sim 169^{\circ}\text{C}$ . All composites displayed a well-form exothermic peak for recrystallization of PVdF at  $\sim 121^{\circ}\text{C}$ . The melting and recrystallization characteristics of PVdF in the composites were substantially identical to those of pure PVdF. In its homogeneous state, poly[4(5)-vinylimidazole/imidazolium trifluoromethylsulfonylimide] exhibited a glass transition temperature,  $T_{g\text{-mid}}$ , of  $-30^{\circ}\text{C}$ . A glass transition temperature was not observed for the poly[4(5)-vinylimidazole/imidazolium trifluoromethylsulfonylimide] phase in the blends, because the temperature was not scanned below  $0^{\circ}\text{C}$  in the DSC thermograms of the blends. Incorporation of benzoyl peroxide resulted in a slight increase in crystallinity of the 3/1 and 4/1 compositions and a substantial increase in crystallinity of the 8/1 composite. Crystallinity increased slightly as the volume fraction of PVdF was increased.

Classic crystalline spherulites were observed in films cast from DMF and dried at temperatures below the melting point of PVdF. On heating to  $200^{\circ}\text{C}$  on the hot stage microscope, crystals melted to reveal a rather amorphous dark field with thin worm-like inclusions which were presumed to arise from the poly[4(5)-vinylimidazole/imidazolium trifluoromethylsulfonylimide] phase. On cooling to ambient temperature, the background field became progressively brighter, however, no structure that might be associated with the reformation of crystallites was observed. This was presumably a result of submicroscopic size of the crystallites.

TGA spectra of the all composite films were characterized by two transitions, one at 300°C corresponding to the decomposition of poly[4(5)-vinylimidazole/imidazolium], and one at 450°C which corresponds to the decomposition of PVdF. Mass loss corresponded well with the mass fractions of the two components of the composite.

Proton conductivity was measured as a function of relative humidity at 80°C. Conductivity (0.05 S/cm) approaching that exhibited by Nafion® 112 (0.18 S/cm) was realized in the 4/1, PVdF/poly[4(5)-vinylimidazole/imidazolium] composite film. Substantial conductivity (0.02 S/cm) was also measured in the 3/1 composite films. No measurable proton conductivity was observed in films of the 8/1 composite. We believe that this is the first instance in which such high proton conductivity levels have been realized in a polymer system where a Grotthuss mechanism of proton transport might be invoked. These results are very exciting and may point the way to the preparation of membranes exhibiting high levels of proton conductivity at elevated temperature and low relative humidity.

## **Acknowledgements**

First of all, I would like to truly thank Dr. Thomas W. Smith as my advisor for his valuable guidance and motivation for both my research and life in RIT. Dr Smith has acted as more like a father to me in the two year-study at RIT. I learned a lot from him and of course will continue to learn things from him after I leave RIT. I would also like to thank Dr. Andreas Langner who has helped me tremendously with his incredible wealth of knowledge. Dr Langner has been a great resource for me when I needed advice.

I would like to thank Dr. Massoud Miri for being my graduate committee member and for all the helpful discussions with him. I would like to extend my thanks to Dr Timothy Fuller at GM Fuel Cell Activities in Honeoye Falls, NY for helping us evaluate the proton conductivity of the composite films. I would like to thank Dr. Benjamin Varela for his help in my stay at RIT.

I would like to give many thanks to Dr K.S.V Santhanam and Dr. Terrence Morrill for financial support from the Materials Science and Engineering Program and from the Department of Chemistry, respectively.

I should also take the opportunity to thank Ms. Brenda Mastrangelo, Mr. Tom Allston and the staff and faculty in chemistry and materials science department who made me have an enjoyable time at RIT.

Heartfelt thanks to my friends and my research team who made these two years easy for me. I extend special thanks to Mufadal Ayubali-Mohamedali, who was a wonderful friend during my stay at RIT.

Family support is very important to me, although most of them are far away from us; so I would like to take this opportunity to thank all my family members. I would like to thank my parents, Xiangju Wu and Xiumei Zhang for all their motivation and love for me in so many years. I would also like to thank my Parents-in-law, Huijun Zhang and Ruifeng Zhao for their supports. Last but not least, I owe many thanks to my beloved wife, Xiaomei Zhang for her love and support without which I would never have reached this point. I have had a wonderful stay at RIT and garnered a lot of sweet memories I will never forget in my life.



### **List of Tables**

Table 1.	Extraction of PVdF/poly[4(5)-VIm/VIm <sup>+</sup> TFSI] Composite Films	21
Table 2.	Extraction of Crosslinked PVdF/poly[4(5)-VIm/VIm <sup>+</sup> TFSI] Composite Films	22
Table 3.	Table of thickness of films before and after annealing at 200°C	23
Table 4	Crystallinity of composite films	32

## List of Figures

Figure 1. Illustration of a PEM fuel cell	1
Figure 2. Structure of Nafion®	2
Figure 3. Structures of poly(arylene ether ketones)	4
Figure 4. Structure of sulfonated polyetheretherketone (S-PEEK)	4
Figure 5. Sulfonated poly(arylene ether sulfone)	5
Figure 6. Grotthus mechanism of proton transport through water molecules	7
Figure 7. Grotthus mechanism of proton transport through imidazole molecules	8
Figure 8. Proton conductivity of poly(4-vinyl-1 <i>H</i> -1,2,3-triazole) and poly-(4-vinylimidazole)	9
Figure 9. Illustration of testing cell	16
Figure 10. Conductivity as a function of the mole fraction of imidazole	18
Figure 11. Picture of a typical composite film dried at 100°C	20
Figure 12. Picture of composite film containing 25 volume % poly[(4(5)-VIm/VIm <sup>+</sup> TFSI](1/0.5) <sub>M</sub> , annealed at 200°C	20
Figure 13. Illustrated positions at which thickness was measured	22
Figure 14. Hot stage micrograph of 3 to 1 film at room temperature	24
Figure 15. Hot stage micrograph of 3 to 1 film at 200°C	24
Figure 16. Hot stage micrograph of 3 to 1 film at room temperature after annealing at 200°C	25
Figure 17. Hot stage micrograph of 4/1 film at room temperature	25
Figure 18. Hot stage micrograph of 4/1 film at 200°C	25
Figure 19. Hot stage microscopy of 4 to 1 film at room temperature after annealing at 200°C	25
Figure 20. Hot stage microscopy of 8 to 1 film at room temperature	26
Figure 21. Hot stage microscopy of 8 to 1 film at 200°C	26
Figure 22. Hot stage microscopy of 8 to 1 film at room temperature after annealing at 200°C	26
Figure 23. Stack plot of heating cycle scans of PVdF	27
Figure 24. Stack plot of cooling cycle scans of PVdF	27
Figure 25. Heating cycle scans in DSC of poly[4(5)-vinylimidazole]	28
Figure 26. Heating cycle scans in DSC of poly[4(5)-VIm/VIm <sup>+</sup> TFSI]	28
Figure 27. Cooling cycle scan in DSC of poly[4(5)-VIm/VIm <sup>+</sup> TFSI]	29

Figure 28. Heating cycle scans in DSC of 3/1 film	29
Figure 29. Cooling cycle scans in DSC of 3/1 film	29
Figure 30. Heating cycle scans in DSC of 4/1 film	30
Figure 31. Cooling cycle scans in DSC of 4/1 film	30
Figure 32. Heating cycle scans in DSC of 8/1 film	30
Figure 33. Cooling cycle scans in DSC of 8/1 film	30
Figure 34. Heat cycle scans in DSC of 3/1 film with dibenzoylperoxide	31
Figure 35. Cooling cycle scans in DSC of 3/1 film with dibenzoylperoxide	31
Figure 36. Heat cycle scans in DSC of 4/1 film with dibenzoylperoxide	31
Figure 37. Cooling cycle scans in DSC of 4/1 film with dibenzoylperoxide	31
Figure 38. Heat cycle scans in DSC of 8/1 film with dibenzoylperoxide	32
Figure 39. Cooling cycle scans in DSC of 8/1 film with dibenzoylperoxide	32
Figure 40. TGA of Poly[(4(5)-VIm/VIm <sup>+</sup> TFSI)]	33
Figure 41. TGA of PVdF	34
Figure 42. TGA of 3/1 PVdF/poly[(4(5)-VIm/VIm <sup>+</sup> TFSI] with 0.1% dibenzoyl peroxide	35
Figure 43. TGA of 4/1 film before crosslinking with dibenzoyl peroxide	36
Figure 44. TGA of 4/1 film after crosslinking with dibenzoyl peroxide	36
Figure 45. TGA of 8/1 film after crosslinking with dibenzoyl peroxide	37
Figure 46. TGA of 8/1 film before cross linking with dibenzoyl peroxide	38
Figure 47. Humidity dependence of conductivity of Nafion®112 at 80° C.	39
Figure 48. Humidity dependence of conductivity of a 3/1 PVdF/poly[(4(5)-VIm/VIm <sup>+</sup> TFSI] composite film at 80°C	39
Figure 49. Humidity dependence of conductivity of a 4/1 PVdF/poly[(4(5)-VIm/VIm <sup>+</sup> TFSI] composite film at 80°C.	40

## Introduction and background

In the present research, composite films of poly(vinylidene fluoride) (PVdF) and poly[4(5)-vinylimidazole/vinylimidazolium (2/1 molar) trifluoromethylsulfonylimide], poly[4(5)-VIm/VIm<sup>+</sup>TFSI<sup>-</sup>], were studied as potential proton exchange membranes for fuel cells.

A proton exchange membrane (PEM) fuel cell, is a device for converting chemical energy into DC electricity and consists of three major components, two electrodes (anode and cathode) separated by a proton exchange membrane. At the anode, hydrogen is oxidized to give an electron and a proton; and at the cathode, oxygen is reduced to give an oxide anion. The electrons produced at the anode are transported, *via* an outer circuit which forms an electric current while the protons are transported, through the PEM, to the cathode where they react with oxygen anions, completing the circuit and the combustion process by producing water. An illustration of a typical fuel cell is showed in Figure 1.

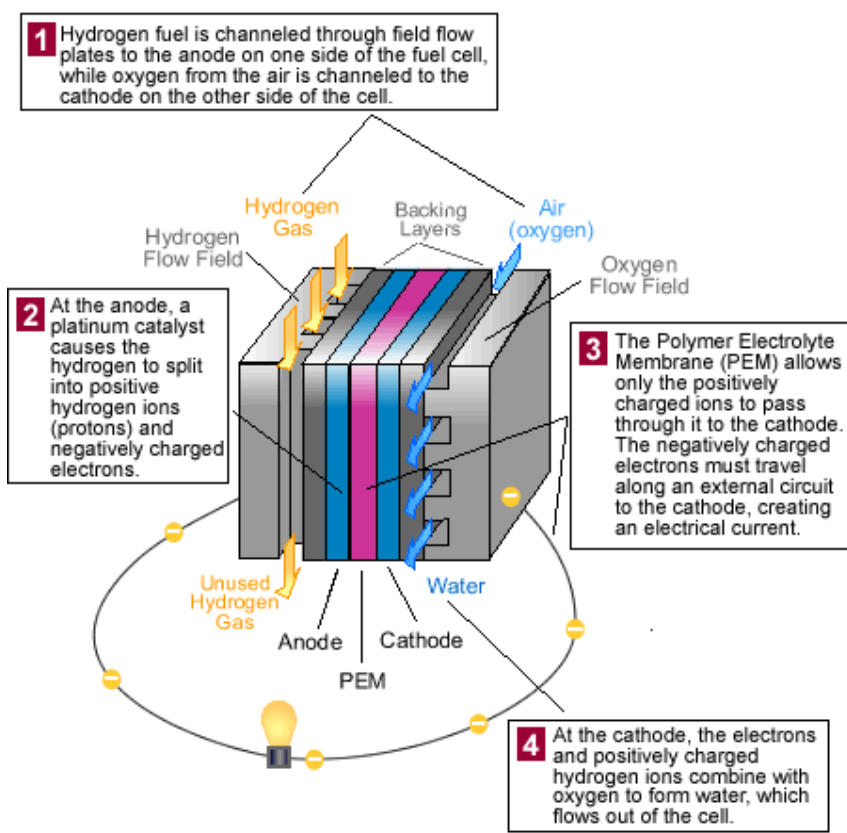


Figure 1. Illustration of a PEM fuel cell<sup>1</sup>

There are many different types of fuel cells, including: phosphoric acid fuel cells (PAFC), proton exchange membrane fuel cells (PEMFC), molten carbonate fuel cells (MCFC), solid oxide fuel cells (SOFC), alkaline fuel cells, regenerative fuel cells, zinc-air fuel cells (ZAFC), and protonic ceramic fuel cells (PCFC)<sup>2</sup>. Among these, proton exchange membrane fuel cells are the most promising device type for application in vehicular systems.

Perfluorosulfonic acid membranes, typified by Nafion® and discovered in the late 1960's by Walther Grot at Dupont<sup>3</sup> are the benchmark proton exchange membranes. Nafion® is a sulfonated tetrafluoroethylene copolymer. The polymer, shown in Figure 2, has a perfluoroethylene backbone with sulfonated perfluoroether side chains.

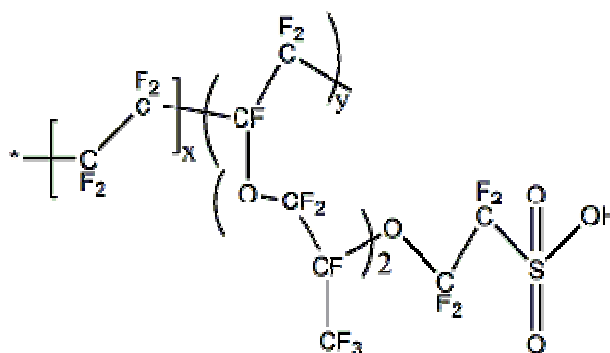


Figure 2. Structure of Nafion

Membrane thickness normally ranges from 25 to 175  $\mu\text{m}$  and proton conductivity in perfluorosulfonic acid polymer membranes is of the order of  $10^{-1} \text{ Scm}^{-1}$  at  $80^\circ\text{C}$  and 100% RH.<sup>4</sup> These fluoropolymer membranes are used in chloro-alkali processing and can withstand harsh thermal-chemical environments. Working life times in fuel cells environment are in excess of >60,000 hours.<sup>5</sup> The excellent thermal, mechanical and chemical/oxidative stability are provided by the tetrafluoroethylene backbone, whilst the sulfonic acid groups provide the proton conductivity.

The critical functional deficiency of perfluorosulfonic acid polymers in PEMs is that proton conductivity in these materials is strongly dependent on the relative humidity. As a result, when operating temperatures exceed  $100^\circ\text{C}$ , water is driven out of the system and the conductivity drops dramatically. In today's engineering prototypes and demonstration vehicles, secondary humidification systems are needed

in order to maintain sufficient conductivity.

Direct methanol fuel cells (DMFC) are proton exchange membrane fuel cells in which the fuel is methanol instead of hydrogen. While perfluorosulfonic acid membranes can be used in DMFCs, they are poor barriers for methanol.

It is desirable to operate fuel cell stacks at elevated temperature because both the H<sub>2</sub>-PEMFC and the DM-PEMFC work better at elevated temperature. The H<sub>2</sub>-PEMFC will tolerate higher levels of carbon monoxide toxication at temperatures in excess of 150°C. In the DM-PEMFC, the kinetics of the methanol oxidation reaction at the anode are faster at temperatures ranging from 130 to 200°C.

The need for a PEM that retains a high level of proton conductivity at elevated temperatures and low RH has become known as the “high temperature membrane problem,”<sup>6</sup> and there has been considerable research in the development of materials that might exhibit significant proton conductivity at low relative humidity, and elevated temperatures. The literature presents at least four generic, materials-based, strategies:

1. Ionomer membranes derived from sulfonated aromatic polymers.
2. Membranes derived from mixtures of polymers containing basic groups (i.e., polybenzimidazole) and strong oxy acids (e.g., phosphoric acid or sulfuric acid).
3. Sulfonic acid ionomer membrane composites with inorganic materials ranging from oxides to lamellar zirconium phosphates or phosphonates.
4. Inert polymers filled with ionomers or inorganic particles possessing high proton conductivity.<sup>7</sup>

#### *Sulfonic acid ionomer membranes*

Aside from fluorosulfonic acid polymer membranes, the predominant types of sulfonated polymer membranes that are being explored as proton exchange membranes are sulfonated poly(arylene ether ketone) membranes and sulfonated poly(arylene ether sulfone) membranes. Poly(arylene ether ketones) are polymers consisting of sequences of ether and carbonyl linkages between phenyl rings. Polyetheretherketone (PEEK) is a typical example which is commercially available (ICI Advanced Materials). Figure 3 displays the structures of poly(ether ketone), PEK,

and poly(ether-ether ketone) PEEK.

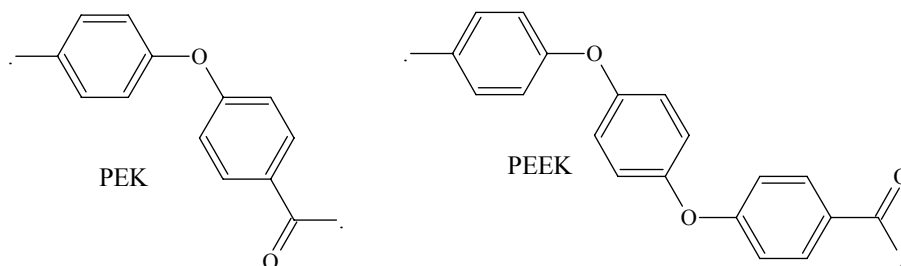


**Figure 3. Structures of poly(arylene ether ketones)**

Sulfonated poly(arylether ketones) may be obtained by sulfonation of preformed polymers or by condensation polymerization of *bis*-phenols with sulfonated aryl ketone precursors.<sup>8</sup> The structure of sulfonated PEEK is shown below in Figure 4.

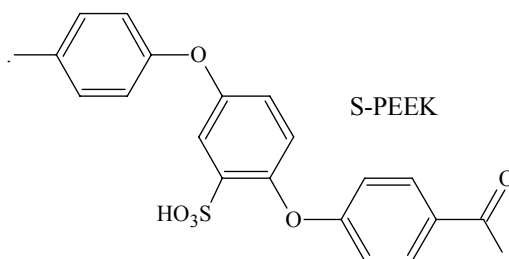


**Figure 4. Structure of sulfonated polyetheretherketone (S-PEEK)**

Sulfonated PEEK can be crosslinked to reduce membrane swelling and increase the mechanical strength of the membrane. Proton exchange membranes derived from sulfonated arylene ether ketones are comparable to commercial Nafion® in terms of their mechanical strength and proton conductivity.<sup>9</sup> However, the conductivity of these kinds of membranes depends on the sulfonation level. When the sulfonation level is high, the polymer becomes soluble in water. The patent literature has claimed that cross-linked and non-cross-linked S-PEEK membranes could offer better performance than Nafion® at elevated temperatures and at lower levels of humidification.<sup>10</sup>

The poly(arylether sulfone) family consists of phenyl rings separated by alternate ether and sulfone ( $-\text{SO}_2-$ ) linkages. Sulfonated derivatives of commercially available poly(arylether sulfone) Udel® (polysulphone, PSU) and Victrex® PES (polyethersulphone, PES) have been extensively studied.

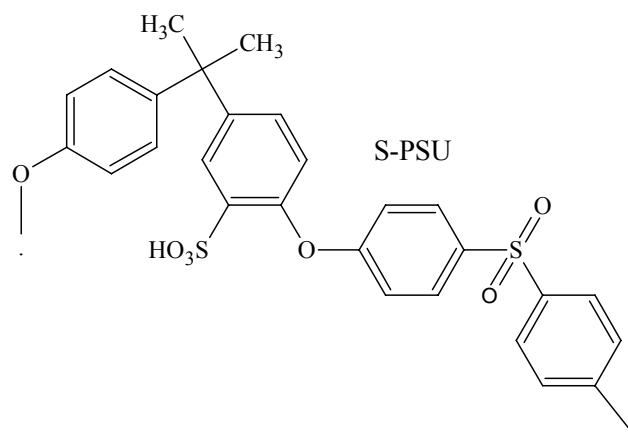


**Figure 5. Sulfonated poly(arylene ether sulfone)**

Proton conductivity in sulfonated poly(arylene ether sulfones) has been reported to be as high as  $4 \times 10^{-2} \text{ Scm}^{-1}$  at  $80^\circ\text{C}$ ;<sup>11</sup> however, conductivity drops dramatically at higher temperatures. Other problems include: excessive water uptake, membrane swelling, loss of mechanical strength and integrity, or even water solubility. To overcome these problems, crosslinking has been tried, however, these deficiencies have not yet been satisfactorily ameliorated.

Poly(4-phenoxybenzoyl-1,4-phenylene) (PPBP) is a relatively new poly(arylene ether ketone) that is being promoted by Maxdem, Inc. (USA) under the trade name Poly-X 2000. Structurally it is similar to PEEK. Sulfonated PPBP is reported to exhibit proton-conductivity at  $80^\circ\text{C}$  as high as  $9 \times 10^{-2} \text{ Scm}^{-1}$ .<sup>12</sup> This is better than that reported for S-PEEK at an equivalent sulfonation level. The higher proton conductivity may be a result of increased water uptake.

Overall, sulfonated polyarylene ethers are less expensive than Nafion®, however their proton conductivity is just as dependent on water content.<sup>13</sup>

#### *Polybenzimidazole/ $\text{H}_3\text{PO}_4$ membranes*

Polymers containing basic ether, amine or imino groups doped with strong acids such as  $\text{H}_3\text{PO}_4$  or  $\text{H}_2\text{SO}_4$ , (particularly polybenzimidazole/ $\text{H}_3\text{PO}_4$  blends) are an extensively studied class of proton exchange membrane materials that have demonstrated good proton conductivity at elevated temperature. Films of polybenzimidazole (PBI) doped with aqueous phosphoric acid have been studied by



Savinell *et al.*<sup>14</sup> They found that the amount of phosphoric acid in the membrane determines the conductivity of the membrane. Conductivity in the range  $5 \times 10^{-3}$  to  $2 \times 10^{-2} \text{ Scm}^{-1}$  was measured at  $130^\circ\text{C}$ . Higher conductivity,  $5 \times 10^{-2} \text{ Scm}^{-1}$ , was found at  $190^\circ\text{C}$ <sup>15</sup>. PBI/ $\text{H}_3\text{PO}_4$  membranes show good mechanical strength up to  $200^\circ\text{C}$ . Mechanical properties are reported to be better than Nafion®<sup>16</sup> Proton conductivity at operating temperatures outlooked for vehicular fuel cell stacks, however, is lower than that for Nafion® systems. Moreover, the durability of PBI/ $\text{H}_3\text{PO}_4$  membranes is poor, due to the fact that  $\text{H}_3\text{PO}_4$  is leached from the membrane. The leached acid can poison electrodes and accelerate their corrosion. The methanol permeability of PBI/ $\text{H}_3\text{PO}_4$  membrane, also is high<sup>10</sup>.

#### *Composites with inorganic materials*

##### Sulfonic acid ionomer membrane composites with inorganic materials ranging from oxides to lamellar zirconium phosphates or phosphonates.

Watanabe, Stonehart<sup>17</sup> and their coworkers reported that Nafion®/ $\text{SiO}_2$  composites were advantageous in the fabrication of  $\text{H}_2/\text{O}_2$  solid polymer electrolyte fuel cells. Antonucci *et al.*,<sup>18</sup> reported the stable operation of a composite Nafion®/ $\text{SiO}_2$ -based liquid-fed direct methanol fuel cell working at  $145^\circ\text{C}$ . Peak power densities of 250 and  $150 \text{ mW/cm}^2$  were achieved in oxygen and air, respectively. Mauritz and coworkers have prepared nanocomposites of Nafion® with  $\text{SiO}_2$ ,  $\text{TiO}_2$ ,  $\text{Al}_2\text{O}_3$ , and  $\text{ZrO}_2$  *via* in situ sol-gel reactions of their respective alkylalkoxysilanes<sup>19,20,21,22,23</sup> and suggested the potential for these nanocomposites as fuel cell membranes. Costamagna and coworkers<sup>24</sup> reported that composite Nafion®/Zirconium phosphate membranes prepared by impregnation of Nafion® 115 or recast Nafion® with zirconyl chloride and 1 M phosphoric acid yielded membrane electrode assemblies that gave 1000-1500  $\text{mA/cm}^2$  at 0.45V and  $130^\circ\text{C}$  and a pressure of 3 bar in a  $\text{H}_2/\text{O}_2$  proton-exchange membrane fuel cell. A problem for these types of membranes might be the reactant cross over.<sup>25</sup>

Inert polymers filled with ionomers or inorganic particles  
possessing high proton conductivity.

Many Attempts to fill the pores of polymeric membranes with finely dispersed precipitates of inorganic proton conductors have been reported. Voids in porous inert polymer such as porous Teflon® can be filled with a solution of a metal (IV) alkoxide. Insoluble metal (IV) hydrous oxide is formed directly inside the membrane pores, by exposing this membrane to wet air. Protonic conductivity of these membranes can be enhanced by treatment with phosphoric acid, which converts the metal (IV) hydrous oxide into its acid phosphate.<sup>7</sup> Alternative treatments between a solution of a zirconyl chloride and phosphoric acid can be used to allow the direct precipitation of amorphous ZrP within the membrane pores<sup>26</sup>. Peled et al.,<sup>27</sup> reported the fabrication of a nanoporous proton-conducting membrane that consists of a ceramic nanopowder (SiO<sub>2</sub>), PVDF and an acid and its application in a direct methanol fuel cell.<sup>28</sup> Nevertheless, the conductivity of this type of membranes is extensively dependent on particle-particle paths connecting the external faces of the membrane. The conduction becomes satisfying only for high contents (>50% V/V) of added particles whereby the strength of the composite membrane becomes a problem.<sup>7</sup>

*Imidazole Systems*

The present research was stimulated by the notion, promoted by Kreuer et al.,<sup>9</sup> that, in imidazole-containing membrane systems, proton transport by a Grotthuss mechanism<sup>29, 30</sup> might enable anhydrous proton conductivity. The Grotthuss mechanism entails the concerted transfer of a proton through a proximate chain of hydrogen-bonded molecules (See Figure 6). Protons can thus be transported at a rate even faster than molecular diffusion.

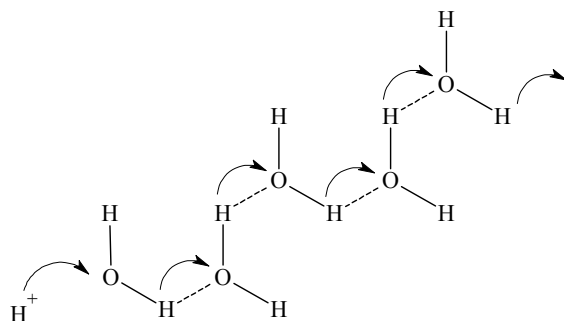


**Figure 6. Grotthuss mechanism of proton transport through water molecules**

Similarly, it would seem that H-bonded sequences of imidazole molecules could transport protons *via* a Grothuss mechanism (see Figure 7 ).

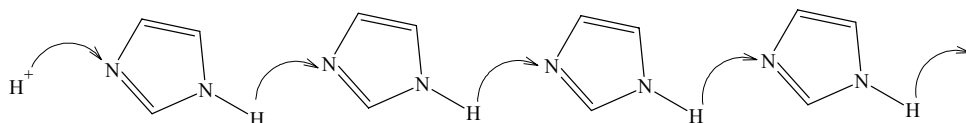


**Figure 7. Grotthuss mechanism of proton transport through imidazole molecules**

Membranes containing imidazoles would therefore be promising materials to employ in a PEM working at elevated temperature if they did indeed exhibit significant proton conductivity by a Grotthuss mechanism.

Meilin Liu and coworkers have extensively studied the possibility of developing triazole containing PEMs. They found that, by imbining 1H-1,2,3-triazole into a sulfonated polysulfone (sPSU) polymer membrane, conductivity up to 0.01 S/cm was realized at 100°C under dry conditions. Because of the low conductivity of sPSU under these conditions, the high conductivity was mainly attributed to triazole. They proposed two conduction mechanisms, long-range translative motion of the triazole groups, and intermolecular proton transfer between adjacent triazole groups. By synthesizing polymers bearing pendant triazole groups, they also showed that proton mobility in triazole polymer was substantially greater than that reported for poly(4-vinylimidazole). Study of cyclic voltammograms (CVs) for 1H-1,2,3-triazole and imidazole showed that triazole has better electrochemical stability than imidazole.<sup>31,32</sup> Figure 8 displays a plot of proton conductivity *versus* temperature for imidazole and triazole polymers presented in the publication by Meilin Liu, et al.<sup>31</sup>

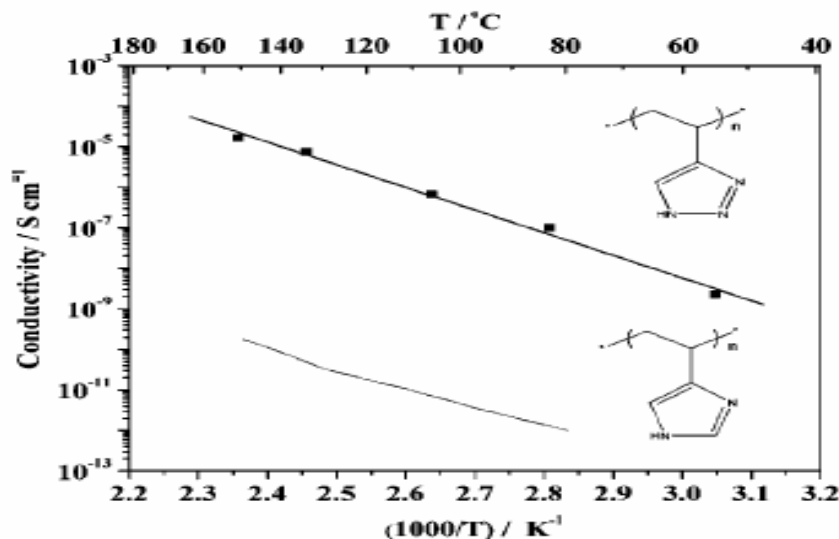


Figure 8.

**Proton conductivity of poly(4-vinyl-1H-1,2,3-triazole) and poly(4-vinylimidazole)**

Both poly[4(5)-vinylimidazole] and poly(4-vinyl-1H-1,2,3-triazole) exhibit some level of proton conductivity however, conductivity exhibited by these polymer is orders of magnitude lower than that provided by fluorosulfonic acid membrane systems.

Rasmussen and coworkers<sup>33</sup> have extensively studied the hydrogen bonding effect on proton mobility in dicyanoimidazole monomer and polymers. They found that both 2-vinyl-4,5-dicyanoimidazole and its polymer are extensively hydrogen bonded and show proton mobility in solid state. Poly(2-vinyl-4,5-dicyanoimidazole) is soluble in a number of polar solvents, including dimethylformamide (DMF), methanol and acetonitrile. Films cast from these solutions were brittle. When films of poly(2-vinyl-4,5-dicyanoimidazole) were annealed, *in vacuo*, at temperatures in excess of 100°C, they became hard and insoluble. By studying the chemical shift trend observed as a function of temperature Rasmussen proposed that poly(2-vinyl-4,5-dicyanoimidazole) has great proton conductivity at high temperatures because of a proton conductivity mechanism which combines “vehicle” (molecular diffusion) and Grotthus (structural diffusion).

Pu, Meyer and Wegner<sup>34</sup> studied proton conductivity of poly[4(5)-vinylimidazole] blended with H<sub>3</sub>PO<sub>4</sub> and H<sub>2</sub>SO<sub>4</sub>. However, the polymer was more than 100% protonated, accordingly conductivity was characteristic of the conductivity of the

respective acids. The conductivity of the blends increased as the temperature was increased. They postulated that proton conductivity in these blends was a result of both proton hopping and polymer segmental movement. As the temperature approached and exceeded the glass transition temperature, segmental motion of the polymer increased, resulting in better conductivity. They also found that the conductivity of poly[4(5)-vinylimidazole] protonated with  $\text{H}_2\text{SO}_4$  was higher than that of poly[4(5)-vinylimidazole] protonated with  $\text{H}_3\text{PO}_4$ . This was ostensibly because  $\text{H}_2\text{SO}_4$  is a stronger acid than  $\text{H}_3\text{PO}_4$ .

Bozkurt and coworkers also investigated the proton conductivity in poly(4-vinylimidazole) protonated with phosphoric acid. They found that poly(4-vinylimidazole) protonated with different level of phosphoric acid was thermally stable up to  $150^\circ\text{C}$ . The glass transition temperature of the poly(4-vinylimidazole) protonated with 200 mole % phosphoric acid was reported to be about  $0^\circ\text{C}$ . The glass transition of the poly(4-vinylimidazole) protonated with 100 mole % of phosphoric acid was  $80^\circ\text{C}$ . A glass transition temperature was not observed in poly(4-vinylimidazole) itself.<sup>35</sup>

Recently, Masayoshi Watanabe and coworkers<sup>36</sup> characterized the melting, ionic conductivity and proton conductivity of the system comprised of *bis*-trifluoromethylsulfonylimide and imidazole under anhydrous conditions. The melting point of the neutral, stoichiometric, salt was  $73^\circ\text{C}$ . The melting points of non-stoichiometric mixtures were lower than that of the equimolar salt. Some were liquid at room temperature. In mixtures with excess imidazole, conductivity decreased with increasing levels of TFSI. Self-diffusion coefficients, measured by pulsed-gradient spin-echo NMR methods, indicated that fast proton exchange was occurring between protonated imidazole cations and neutral imidazole moieties. Proton conduction was presumed to occur by a combination of Grotthuss and vehicle-type mechanisms. Proton conduction was confirmed by direct current polarization measurements. Reduction of molecular oxygen was observed at the interface between a Pt electrode and IM/TFSI ionic liquids.

Fuller and coworkers<sup>37</sup> developed ionically conductive, rubbery gel electrolytes

comprised of copoly(vinylidene fluoride/hexafluoropropylene) PVdF/HFP plasticized with room temperature ionic liquid imidazolium salts. Ionic conductivity levels as high as 1.1-5.8 mS/cm at room temperature were reported. These conductive gel electrolytes, based on ionic liquid imidazolium salts and PVdF/HFP, are nonvolatile and thermally stable and were successfully operated at temperatures up to 200°C.

We chose to study PVdF/poly[4(5)-vinylimidazole/imidazolium trifluoromethylsulfonylimide] composites because;

1. the close proximity and high volume density of imidazole groups, poly[4(5)-vinylimidazole] or block copolymers thereof were thought to offer an excellent platform for maximizing proton conductivity by a Grotthuss mechanism.
2. PVdF is a soluble, melt-processible, polymer that has excellent chemical/oxidative and thermal stability.
3. as was reported by Fuller, PVdF can be plasticized by small molecular quaternary imidazolium room temperature ionic liquids, and
4. Watanabe et al. demonstrated significant proton conductivity in fractionally protonated imidazole systems.

## **Experimental**

### *Materials*

Urocanic acid (99%), iodomethane (99%), picric acid, dimethylsulfate (99%), 1,1,1,3,3,3-Hexamethyldisilazane (98%), and dibenzoyl peroxide were obtained from Acros Organics. Chloroform (99.8%), 4-methoxyphenol (99%), trifluoromethanesulfonylimide (TFSI) (95%), and 4-methoxyphenol (99%) were purchased from Aldrich Chemical Company Inc. Milwaukee, WI. N,N'-dimethylformamide (DMF) was purchased from SIGMA Chemical Co. St. Louis, MO. Pentane, potassium hydroxide pellets (Baker Analyzed), potassium carbonate (anhydrous), EMD chemicals Inc, benzene Tokyo Kasei Kogyo Co. Ltd. and ethyl alcohol Pharmco products Inc (absolute anhydrous) were purchased through VWR, Bridgeport, NJ. Kynar® 301F poly(vinylidene fluoride), was obtained from Atochem North America, Inc..

#### *4(5)-vinylimidazole*

4(5)-vinylimidazole was prepared by decarboxylation of urocanic acid in accordance with the procedure published by Overberger et al.<sup>38</sup> Thus, 1.72 grams of anhydrous urocanic acid was charged to a short path distillation apparatus. The apparatus was then immersed in a 220°C oil bath and 4(5)-vinylimidazole distilled over under vacuum over a period of four and a half hours. The crude monomer crystallized upon refrigeration for 48 hours, yielding 0.77 grams (65.7% yield) of product. Crude 4(5)-vinylimidazole was purified by sublimation. In a typical purification process, 2 grams of 4(5)-vinyl imidazole was placed in a small sublimator. The system was evacuated and immersed in a 70°C oil bath. White quickly formed on the cold finger and after 4 hours 1.78 grams (89 %) of pure 4(5)-vinyl imidazole was collected. The monomer was stored in a freezer at ~0°C.

#### *Polymerization of 4(5)-vinylimidazole in benzene solution*

1.25 grams (13 mmol) of sublimed 4(5)-vinyl imidazole and 0.02 grams (0.12 mmol) of azo-bis-isobutylnitrile (AIBN) were dissolved in 10 ml benzene and placed in a sealed tube. The monomer solution was degassed by subjecting the material in the tube to at least three evacuation, freeze and thaw cycles. After the final freeze thaw cycle, the contents of the tube were frozen and the tube was sealed. The sealed polymerization tube was then placed in a 65°C oil bath for 48 hours. Polymer precipitated from the benzene solution as it was formed. Upon completion of the polymerization, the tube was opened, benzene was decanted and the polymer was dissolved into 10 ml methanol. Poly(4,5-vinylimidazole) was reprecipitated in benzene by drop wise addition of the methanol solution in 150 ml of benzene yielding 1.9 grams of pure poly[4(5)-vinylimidazole] which was collected by filtration.

#### *Polymerization of 4(5)-vinylimidazole in ethanol/water solution*

1 gram (10.6mmol) of sublimed 4(5)-vinylimidazole was dissolved in 10ml ethanol/water solution (1 to 1). 4,4-azobis(4-cyano-valeric acid), 0.014 grams, was

added to the solution and the solution was then charged to a Carius tube. The tube was subjected to three freeze-thaw cycles, sealed *in vacuo*, and immersed in a 65°C oil bath for ~16 hours. A clear viscous solution was obtained. The polymer ethanol/water solution was put into a 2000 molecular weight cut-off dialysis bag. The membrane was tied and the bag was tied, placed in a Soxhlet extractor and extracted with refluxing benzene for 48 hours. Poly[4(5)-vinylimidazole] precipitated in the bag as benzene diffused in. After drying in an evacuated desiccators, 0.6 grams of pure poly[4(5)-vinylimidazole] was collected.

#### *15 Weight % solution of PVdF in DMF*

A 15% by weight solution of PVdF in DMF was prepared by dissolving 2 grams of kynar®301 into 13.5 ml DMF.

#### *15 Weight % solution of poly[4(5)-vinylimidazole] in DMF*

2.2 grams (23.4 mmol) of poly[4(5)-vinylimidazole] {poly[4(5)-VIm]} was charged to a disposable test tube. 3.36 grams (11.7 mmol) of trifluoromethylsulfonylimide (TFSI) was added to the test tube along with 15 ml DMF to yield a homogeneous solution of poly[4(5)-vinylimidazole/imidazolium(2:1molar)] {poly[(4(5)-VIm/VIm<sup>+</sup>TFSI)(1/0.5)<sub>M</sub>]}.

#### *PVdF/poly[(4(5)-VIm/VIm<sup>+</sup>TFSI)] composite films*

##### PVdF/poly[4(5)-VIm/VIm<sup>+</sup>TFSI](1/0.5)<sub>M</sub>]<sub>(3/1)<sub>v</sub></sub>

A homogenous composite solution was made by mixing 3 ml of the 15% Weight % solution of PVdF in DMF with 1 ml of 15 Weight % solution of poly[4(5)-vinylimidazole] in DMF. Films were prepared by drawdown casting onto a 5" x 7" glass plate mounted on a perforated vacuum drawn down table which was covered with a sheet of 1024 bond paper. Thus, the gap of an adjustable drawn wedge (doctor blade) was set at 20 mil and 4 ml of the composite solution was drawn down. It was anticipated that the thickness of the resultant, dried film would be about 50 μm. After the film was dried at room temperature for an hour, it was annealed on a hot plate annealing at 100°C for 24 hours to yield an



opaque white film. This process was repeated to prepare several films. Some of the films, initially dried at 100°C for 24 hours, were subsequently heated, under Ar, at 200°C for 5 min. The effect of being heated to 200° C was that the films became substantially transparent. The average thickness of the films dried at 100°C was 0.0045inches. After heating to 200°C, the average thickness was 0.0015 inches.



Films of the above composition were prepared by an analogous procedure to that used to prepare the (3/1)<sub>v</sub> composite. The average thickness of the films dried at 100°C was 0.0040 inches. After heating to 200°C, the average thickness was 0.00175 inches.



Films of the above composition were prepared by an analogous procedure to that used to prepare the (3/1)<sub>v</sub> composite. The average thickness of the films dried at 100°C was 0.0045inches. After heating to 200°C, the average thickness was 0.0015 inches.

#### Crosslinked PVdF/poly[4(5)-VIm/VIm<sup>+</sup>TFSI](1/0.5)<sub>M</sub>] composite films

Dibenzoylperoxide was added to (3/1), (4/1) and (8/1)<sub>v</sub> solutions of PVdF/poly[4(5)-vinylimidazole/imidazolium 2:1 molar in DMF in order to promote crosslinking within the film. Peroxide was incorporated at two levels 1% and 0.1%. The peroxide-doped films were dried at lab ambient temperature for one hour and directly heated at 200°C, under Ar, for 5 minutes. The compositions containing 0.1% by weight of peroxide became substantially transparent, just like those that were not doped with peroxide. The compositions doped at 1% by weight of peroxide cracked after they were annealed at 200°C.

#### *Characterization of the composite films*

##### Differential Scanning Calorimetry (DSC)

DSC analysis was conducted on a TA instruments DSC 2010 with a low temperature measuring head and liquid nitrogen cooled heating element. Sample

pans were heated and cooled at a rate of 10°C/min. All the samples were subjected to multiple heating and cooling cycles. Protonated poly[4(5)-vinylimidazole], pure PVdF, and films with 3 different polymer compositions before and after annealing at 200°C were studied by DSC.

#### Thermal gravimetric analysis (TGA)

TGA of all the samples were carried out on a TGA 2050 thermal gravimetric analyzer. The typical running process for TGA here is first heating up the materials to 800°C at a rate of 10°C/min and then holding the temperature at 800°C for 2 minutes. The protonated poly[4(5)-vinylimidazole], pure PVdF, and films with 3 different polymer compositions before and after annealing at 200°C were studied by TGA

#### Polarized, hot-stage microscopy

Polarized hot-stage microscopy was carried out on a Nikon Eclipse E600 POL with an INSTRON STC200 temperature control stage. The samples were heated and cooled from 0°C to 200°C at a rate of 10°C/minutes. Micrographs were taken every 10 minutes.

#### Conductivity Measurements

The conductivity was evaluated in a fuel cell test fixture at 80°C and at relative humidity (RH) levels ranging from 0 -100% RH. Proton conductivity was evaluated by Dr Timothy Fuller at General Motors Global Alternative Propulsion Center, Honeoye Falls, NY. Electrical resistance was measured in the in-plane direction of the membrane with varied relative humidity and temperature. The apparatus consisted of a 4-point probe, with an a direct current applied *via* a computer assisted Gamry card serving as a potentiostat and using a BakkTech cell (Loveland, CO) with a 5-cm<sup>2</sup>, straight-flow-field made of Poco graphite, with heated metal end-plates (Fuel Cell Technologies hardware). The membrane sample size was 0.9 cm x 4.5 cm. The hardware was equipped with an external humidifier. Membrane thickness was measured using a Mitutoyo micrometer. A d.c. voltage sweep was applied over the range between 0.05 and 0.6V, across the inner electrodes (sense and reference) by increasing current at the outer probes (working

and counter). The current  $i$  was measured and plotted against voltage, and the slope of the line was the sample resistance. Measurements of conductivity were made as function of percent relative humidity and temperature, usually at 80°C. Dry membrane thickness was measured with a micrometer and this value was used in the conductivity calculations.

$$R = \text{resistivity } (\rho) \times L/A = (V_a - V_b)/R = V_{ab}/R$$

The electrical conductivity,  $\sigma$ , of a material is the reciprocal of  $\rho$  and  $i = \sigma A (V_a - V_b)/L$ , where  $L$  is the distance between 2 points on a conductor and  $i/A$  is the current per unit cross-sectional area.

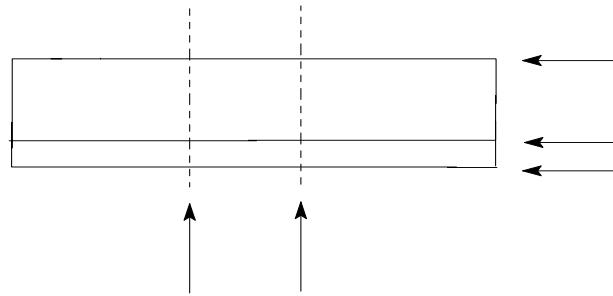


**Figure 9. Illustration of testing cell**

Resistance in terms of bulk resistivity is:

$$R = \rho L/A = \rho L/(WT)$$

$$\rho = RWT/L$$

$$\sigma = 1/\rho = L/(RWT)$$

A piece of membrane (0.9 cm x 4.5 cm) was die-cut from the as-received membrane using a custom-made Paragon die. The membrane was placed in a BekkTech conductivity cell with platinum electrodes set-up as a 4 point probe. The BekkTech cell was placed in fuel cell hardware with graphite straight flow field design with heaters and temperature control set at 80°C, and a humidifier maintained the relative humidity at a predetermined set point between 20 and 100% relative humidity. The flow of hydrogen was 2 standard liters per minute. A Gamry Instruments potentiostat card, installed in a lab-grade personal computer, was used for the DC conductivity measurements. The applied voltage sweep

across the inner electrode probes (sense and reference) was performed over the range from 0.05 to 0.6 V by increasing the current across the outer electrodes (working and counter). The current was simultaneously measured and plotted against voltage. The slope of the plot yielded the sample resistance. Conductivity was determined with relative humidity at 10% relative humidity increments starting at 20% and ending at 100% relative humidity. Equilibration times at the respective relative humidity values was greater than 30 minutes. In the case of the specific PVDF samples, conductivity was measured from 100% to 20% relative humidity and then back up, from 20% to 100% relative humidity. The high relative humidity values did not repeat, suggesting there are issues with membrane stability. Lower conductivity at 100% relative humidity in the repeat measurements suggests that the conducting species might be washing out of the membrane.

#### *Nuclear magnetic resonance (NMR)*

Nuclear magnetic resonance or NMR was used to confirm the structure of vinylimidazoles synthesized in this research. The NMR was carried out on a Bruker 300Hz NMR.

## Results and discussions

In order to demonstrate proton conductivity in an imidazole polymer system, novel composite proton exchange membranes were fabricated by casting composite films of poly[4(5)-vinylimidazole/vinylimidazolium trifluoromethylsufonylimide] {[poly[4(5)-VIm/VIm<sup>+</sup>TFSI](1/0.5)<sub>M</sub>]} and poly(vinylidene fluoride), PVdF, from mixed dimethylformamide, DMF, solutions. The phase composition and morphology of these composites were examined by differential scanning calorimetry, and polarized hot-stage microscopy. Thermal stability was evaluated by TGA. Proton conductivity was evaluated at GM Fuel Cell Activities in Honeoye Falls, NY. The present work differs from that which was previously done in poly[4(5)-vinylimidazole] systems in that previous researchers either examined films of the neutral polymer<sup>39</sup> or systems in which poly[4(5)-vinylimidazole] was used as a basic polymer medium in which an excess of protic acid was dissolved.<sup>34</sup> These systems were essentially variants of the liquid protic acid fuel cell systems<sup>35</sup> in which electrolyte bleed is a debilitating problem.

The reports by Watanabe and Susan et al.,<sup>17</sup> in which significant levels of proton conductivity ( $\sim 0.1$  S/cm at 130°C) were measured in ionic liquid compositions comprised of imidazole fractionally protonated with trifluoromethylsufonylimide, stimulated us to examine fractionally neutralized poly[4(5)-vinylimidazole] systems.

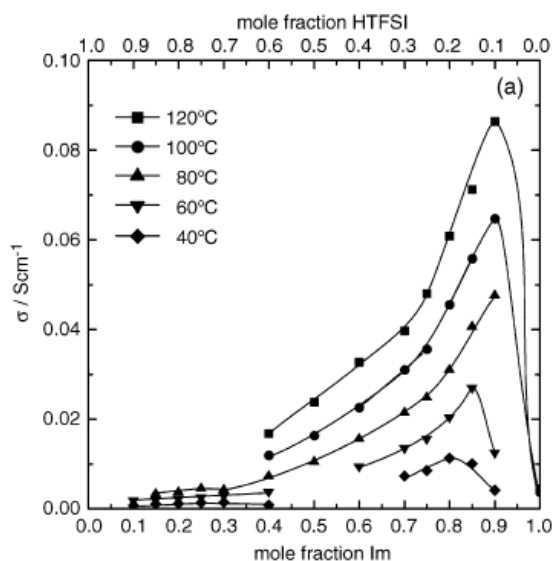


**Figure 10. Conductivity as a function of the mole fraction of imidazole**

Figure 10, was taken from Susan and Watanabe's, 2004 J Phys. Chem. paper and shows that the ionic conductivity of the imidazole/TFSI system was maximized at a neutralization fraction of about 0.10. While the fractionally neutralized liquid ionic system exhibited high proton conductivity, its utility in a practical membrane electrode assembly, would be limited by issues of containment and bleed like those encountered in liquid protic acid systems.<sup>40</sup>

In order to facilitate dissolution in DMF, poly[4(5)-vinylimidazole] was protonated with 50 mole percent of TFSI. Films of poly[(4(5)-VIm/VIm<sup>+</sup> TFSI)(1/0.5)<sub>M</sub>], however, were tacky, gooey resinous materials. DSC analysis indicated a glass transition of ~-30°C. In order to enhance mechanical strength, a polymer blend strategy was adopted. PVdF is soluble in DMF and has been shown to be a chemically stable and thermally stable material with good mechanical and gas permeability properties.<sup>37</sup> Accordingly, it was chosen as the film-forming matrix in our composites. Homogenous solutions of PVdF/poly[(4(5)-VIm/VIm<sup>+</sup> TFSI)(1/0.5)<sub>M</sub>] in DMF were prepared and films were cast therefrom. Films were cast from DMF solutions with different volume fractions of PVdF and poly[(4(5)-VIm/VIm<sup>+</sup> TFSI)(1/0.5)<sub>M</sub>]. Films were characterized by DSC, polarized light microscopy (PLM), and TGA. Conductivity was evaluated by Dr Timothy Fuller at General Motors Global Alternative Propulsion Center, Honeoye Falls, NY.

#### *A. Fabrication of PVdF/poly[4(5)-vinylimidazole/imidazolium TFSI] composite films*

As was described in the Experimental Section, composite films were cast from DMF solutions of poly[(4(5)-VIm/VIm<sup>+</sup> TFSI)] and PVdF. Three compositions were prepared in which the volume fraction of PVdF was 0.66, 0.75 and 0.89, respectively. After the films were dried at room temperature for an hour, they were put on a hot plate and dried at 100°C for 24 hours. Opaque, white films, like that showed in Figure 11, were obtained with all three compositions.



**Figure 11. Picture of a typical composite film dried at 100°C**

The films were brittle and had little mechanical strength. However, on annealing under Ar, at 200°C for a mere 5 minutes, the films became transparent and strong. The annealed composite film with the highest poly[(4(5)-VIm/VIm<sup>+</sup> TFSI)(1/0.5)<sub>M</sub>] content (25 volume %) is shown in Figure 12.



**Figure 12. Picture of composite film containing 25 volume % poly[(4(5)-VIm/VIm<sup>+</sup> TFSI)(1/0.5)<sub>M</sub>], annealed at 200°C**

Given the fact that PEMs must work in a humidified environment and the water solubility of protonated poly[4(5)-VIm], it was suspected that the protonated poly[4(5)-VIm] might be extracted from the composite films by water. Accordingly, all films were weighed, extracted with distilled water for 48 hours at ambient

temperature and dried to constant weight. The 8/1, 4/1 and 3/1 films lost 16.7, 26.1 and 30% of their original mass, respectively. The data is summarized in Table 1

PVdF/poly[4(5)-VIm/VIm <sup>+</sup> TFSI] ratio	Original mass (g)	Final mass (g)	Percent Mass lost
8 to 1	0.0168	0.0140	16.7%
4 to 1	0.0337	0.0249	26.1%
3 to 1	0.0447	0.0313	30.0%

**Table 1. Extraction of PVdF/poly[4(5)-VIm/VIm<sup>+</sup>TFSI] Composite Films**

Clearly, almost all of the poly[4(5)-VIm/VIm<sup>+</sup> TFSI] was extracted. For the 8 to 1 composite, complete extraction of poly[4(5)-VIm/VIm<sup>+</sup> TFSI] would result in a 12.5% weight loss; a 16.7% weight loss was measured. For the 4 to 1 composite, complete extraction of poly[4(5)-VIm/VIm<sup>+</sup> TFSI] would result in a 25% weight loss; a 26.1% weight loss was measured. For the 3 to 1 composite, complete extraction of poly[4(5)-VIm/VIm<sup>+</sup> TFSI] would result in a 33% weight loss; a 30% weight loss was measured.

In order to prevent extraction of the protonated imidazole polymer by water, we attempted to crosslink the composite films. Dibenzoyl peroxide was used to generate free-radicals. Two sets of films were cast from DMF solutions of PVdF/poly[4(5)-VIm/VIm<sup>+</sup> TFSI] doped with 1 mole % and 0.1 mole % dibenzoyl peroxide. The films were dried at ambient temperature in air for 4 hours, heated at 70°C for 2 hours and annealed at 200°C for 5 minutes. The set of composite films doped with 1 mole % dibenzoyl peroxide were extensively cracked, an apparent result of substantial crosslinking. The appearance of the set of composite films doped with 0.1 mole % of dibenzoyl peroxide was identical to that of films cast without peroxide. They were transparent and strong and no cracks could be detected by the naked eye. This set of films was extracted with water as in the protocol described above for the peroxide-free films. The 8/1, 4/1 and 3/1 films lost 2.6%, 3.1% and 7.6% of their original mass,



respectively. The data is summarized in Table 2.

PVdF/poly[4(5)-VIm/VIm <sup>+</sup> TFSI] ratio	Original mass(g)	Final mass (g)	Percent Mass lost
8 to 1	0.0234	0.0228	2.6%
4 to 1	0.0310	0.0298	3.1%
3 to 1	0.0367	0.0339	7.6%

**Table 2.**

**Extraction of Crosslinked PVdF/poly[4(5)-VIm/VIm<sup>+</sup>TFSI] Composite Films**

Clearly crosslinking films reduced the mass loss upon water extraction of the composite films. It thus appears that robust composite films in which protonated poly[4(5)-vinylimidazole] is substantially fixed and immobilized can be realized by simply incorporating a small amount of peroxide in the film prior to drying and annealing.

The thicknesses of the composite films were compared before and after annealing at 200°C. The thickness of each film was measured in the 5 positions shown in Figure 13

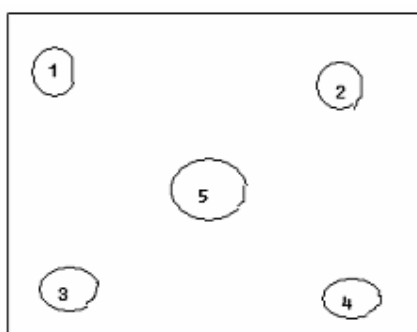


**Figure 13. Illustrated positions at which thickness was measured**

The measured thicknesses of the crosslinked films before annealing are summarized in Table 3.

PVdF/poly[4(5)-VIm/VIm <sup>+</sup> TFSI] ratio	Film thickness at specified position in mils Before/After annealing				
	1	2	3	4	5
8 to 1	4.75/1.5	5.0/1.5	4.0/1.4	4.25/1.5	4.0/1.5
4 to 1	4.0/1.75	4.1/2.0	3.5/1.5	4.0/1.75	3.6/1.75
3 to 1	4.5/1.0	4.6/1.2	4.5/1.5	4.4/1.5	4.2/1.5

**Table 3. Table of thickness of films before and after annealing at 200°C**

Annealing at 200°C resulted in a significant, 300%, reduction in the thickness of the films. Given no apparent change in the dimensions of films that were thoroughly dried at 100°C prior to annealing at 200°C and the substantially increased strength and clarity of the annealed films, it might be reasonably concluded that the thinning of the films was a result of densification.

#### *B. Characterization of the composite films*

The composition and morphology of composite films were examined by differential scanning calorimetry and polarized hot-stage microscopy. Stability at elevated temperature was assessed by thermal gravimetric analysis.

##### 1. Polarized light microscopy (PLM)

Hot-stage, polarized light microscopy was used to examine the changes of morphology of the composite films. Polarized light microscopy is a technique used to reveal anisotropic properties of materials. In this research, crystallites are anisotropic and the amorphous component is dark under polarized microscope. Figure 14 displays a polarized micrograph of a film cast, at room temperature, from the 3 to 1 by volume PVdF/poly[4(5)-VIm/VIm<sup>+</sup>TFSI] polymer blend. The inset picture in the top left corner of Figure 14 shows an unmagnified picture of that film. The dark areas in the polarized micrograph are ostensibly amorphous regions perhaps rich in poly[4(5)-VIm/VIm<sup>+</sup>TFSI]; the bright birefringent areas must be substantially comprised of crystalline PVdF.

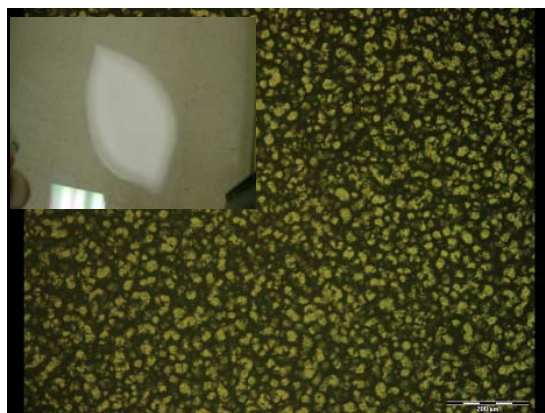


**Figure 14. Hot stage micrograph of 3/1 film at room temperature**

When this film was heated to 200°C, at a rate of 10°C per minute, and held at 200°C for 5 minutes; its hot-stage micrograph changed to appear as shown in Figure 15. At this point, the PVdF crystals have apparently melted and one sees a somewhat brighter, but still darkened, field typical of an amorphous melt, with brighter worm-like inclusions.

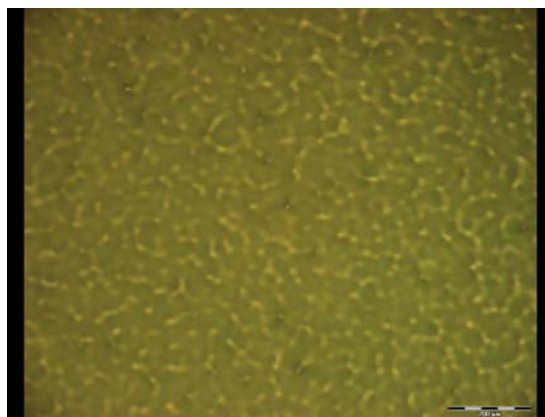


**Figure 15. Hot stage micrograph of 3 to 1 film at 200°C**

After cooling to ambient temperature at a rate of 10° per minute, the polarized micrograph shown in Figure 16 was obtained. The field in this micrograph is quite bright.

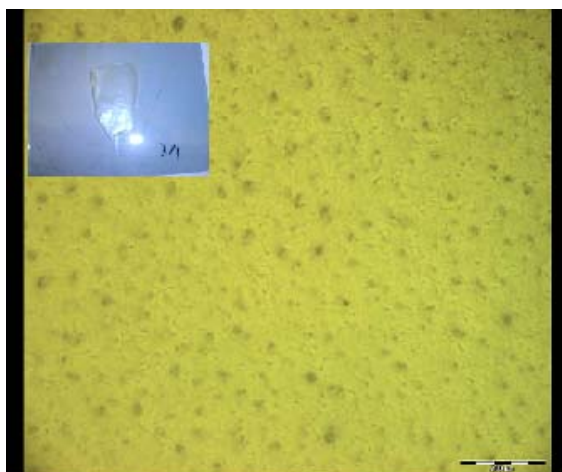


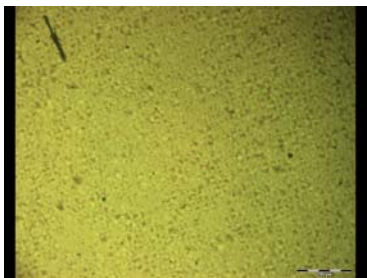
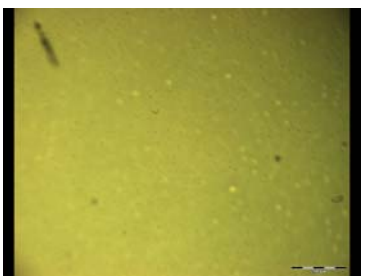
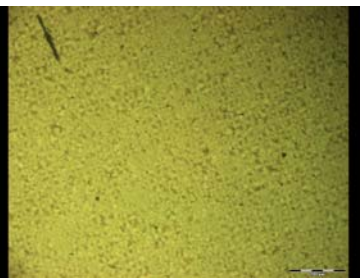
**Figure 16. Hot stage micrograph of 3 to 1 film at room temperature after annealing at 200°C**

The picture inset in the top left corner of Figure 16 shows what the film looks like to the naked eye after it was annealed at 200°C for 5 minutes. The film now is clear and a lot stronger than it was before annealing. The bright field of the polarized light micrograph is presumably a result of the fact that sub-microscopic crystals are uniformly dispersed in this film.

Similar behavior was observed in hot-stage micrographs of the 4 to 1 PVdF/poly[4(5)-VIm/VIm<sup>+</sup> TFSI] polymer blend (shown in Figures 17-19).

<p><b>Figure 17</b> Hot-stage micrograph of 4/1 film at room temperature</p>	<p><b>Figure 18</b> Hot-stage micrograph of 4/1 film at 200°C</p>	<p><b>Figure 19</b> Hot-stage micrograph of 4/1 film at room temperature after annealing at 200°C</p>

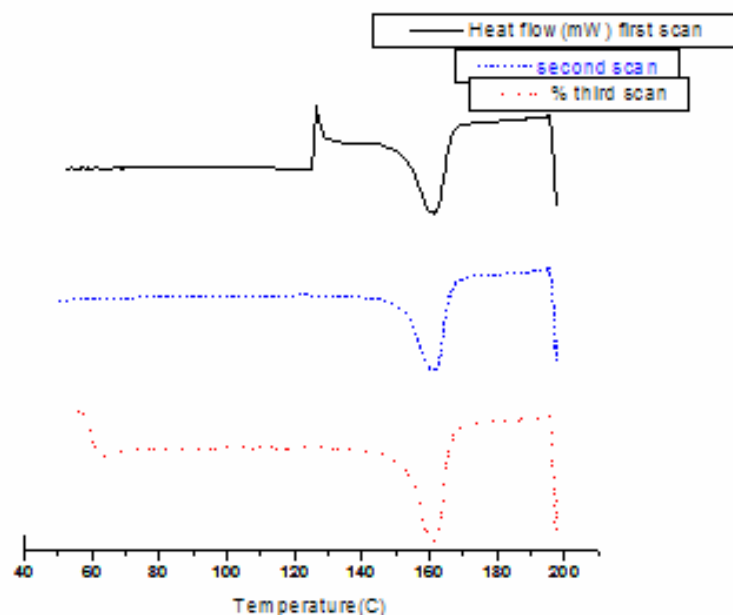
In the hot-stage micrographs of the 8/1 blend (shown in Figure 20-22), little change was seen in the before and after the annealing micrographs. This is ostensibly a result of the small volume fraction of poly[4(5)-VIm/VIm<sup>+</sup> TFSI] in the 8/1 blend.

		
<b>Figure 20</b> Hot-stage micrograph of 8/1 film at room temperature	<b>Figure 21</b> Hot-stage micrograph of 8/1 film at 200°C	<b>Figure 22</b> Hot-stage micrograph of 8/1 film at room temperature after annealing at 200°C

Hot-state microscopy of the films cast from the 3/1 by volume PVdF/poly[4(5)-VIm/VIm<sup>+</sup>TFSI] polymer blend doped with 0.1% dibenzoylperoxide yielded micrographs that were similar to those obtained with the peroxide-free 3/1 composite.

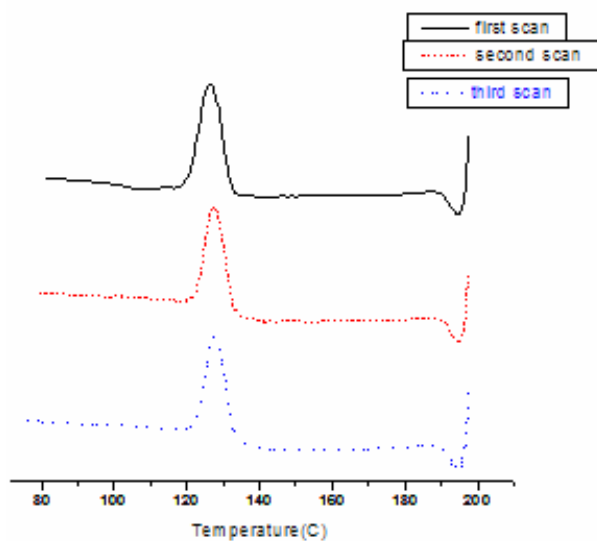
## 2. Differential Scanning Calorimetry (DSC)

PVdF is a well-studied semicrystalline polymer and exhibits a crystalline melt at 166-170°C<sup>41</sup>. In carrying out our DSC analyses, a typical protocol was to first ramp to 60°C and cool to 0°C at a rate of 20°C/minute. The sample was then ramped to 200°C at a rate of 10°C/minute and held at 200°C for 5 minutes. The sample was then cooled to 0°C at a rate of 10°C/minute and held at 0°C for 5 minutes. Thus, the first scan was completed. This cycle was repeated until two DSC traces overlapped, being virtually identical. Figures 23 and 24 display stack plots of heating and cooling curves for three DSC cycles of pure PVdF.



**Figure 23. Stack plot of heating cycle scans of PVdF.**

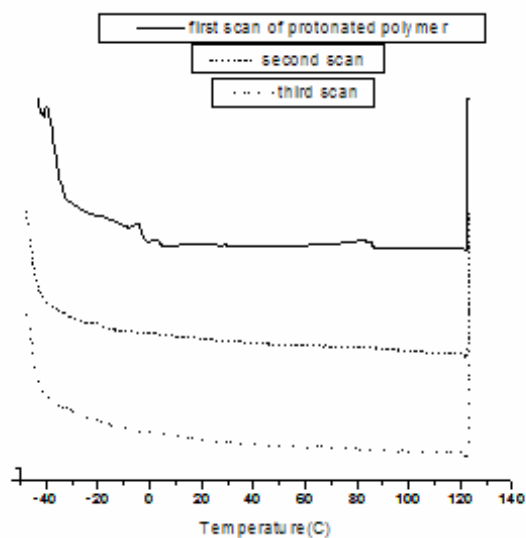
The melt endotherms in the three DSC heating cycle scans of PVdF, shown in Figure 23, overlap and indicate a melting point of  $\sim 167^{\circ}\text{C}$ .



**Figure 24. Stack plot of cooling cycle scans of PVdF**

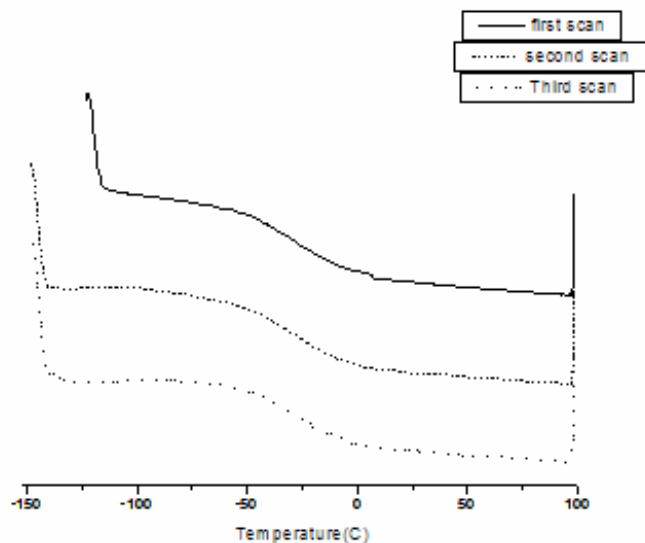
The crystallization exotherms in the three DSC cooling cycle scans of PVdF, shown in Figure 24, overlap and indicate recrystallization at a peak temperature of  $127^{\circ}\text{C}$ .

Poly[4(5)-vinylimidazole] is an amorphous polymer and would be expected to exhibit a glass transition. However, Figure 25 shows no glass transition in the DSC of poly[4(5)-vinylimidazole] in the temperature range between 50 and 200°C.



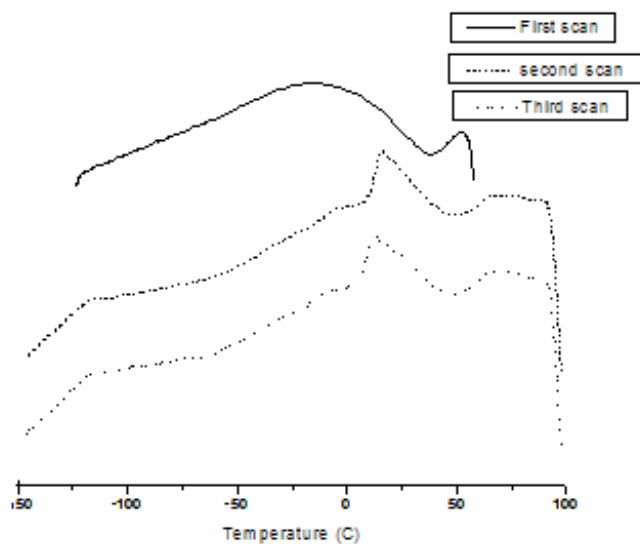
**Figure 25. Heating cycle scans in DSC of poly[4(5)-vinylimidazole].**

Figure 26 displays DSC heating cycle scans of poly[4(5)-VIm/VIm<sup>+</sup>TFSI] in the temperature range from -150°C to 100°C. There is an apparent glass transition, T<sub>g</sub>-(mid), at around -50°C.



**Figure 26. Heating cycle scans in DSC of poly[4(5)-VIm/VIm<sup>+</sup> TFSI]**

Figure 27 shows DSC cooling cycle scans for the poly[4(5)-VIm/VIm<sup>+</sup>TFSI]. Scans 2 and 3 are nearly identical and differ from the first cooling scan. One can see that there is an exothermic peak, reminiscent of a recrystallization event, at about 10°C in the second and third cooling scans. The origin of this exothermic peak is not known.



**Figure 27. Cooling cycle scan in DSC of poly[4(5)-VIm/VIm<sup>+</sup>TFSI]**

In the series of figures which follow, DSC heating and cooling curves for composite films cast from DMF solutions of poly[(4(5)-VIm/VIm<sup>+</sup>TFSI] and PVdF are displayed. The features in the DSC thermograms of the composites are analogous to those of pure PVdF, i.e., a melting endotherm at about 167°C and a recrystallization exotherm peaking at about 125°C.

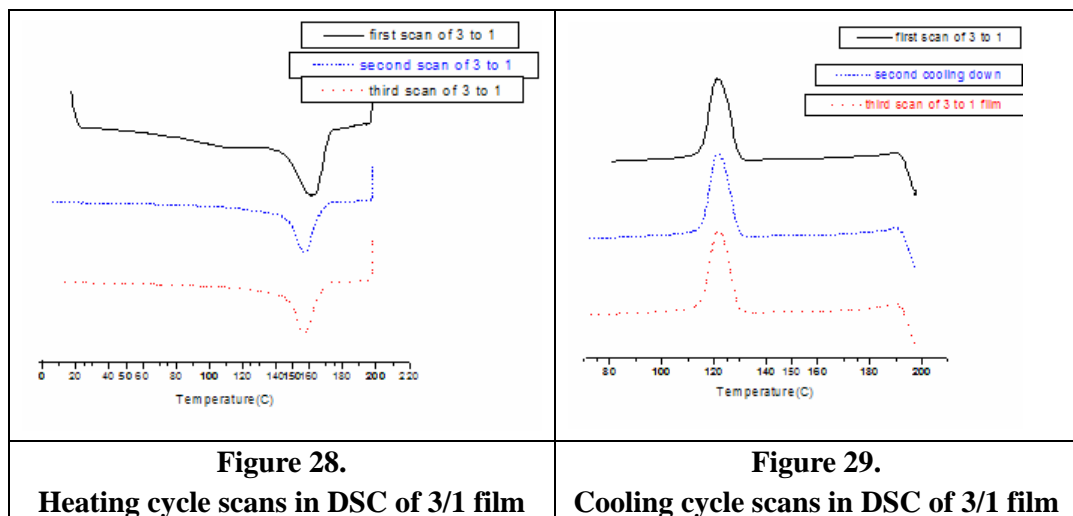
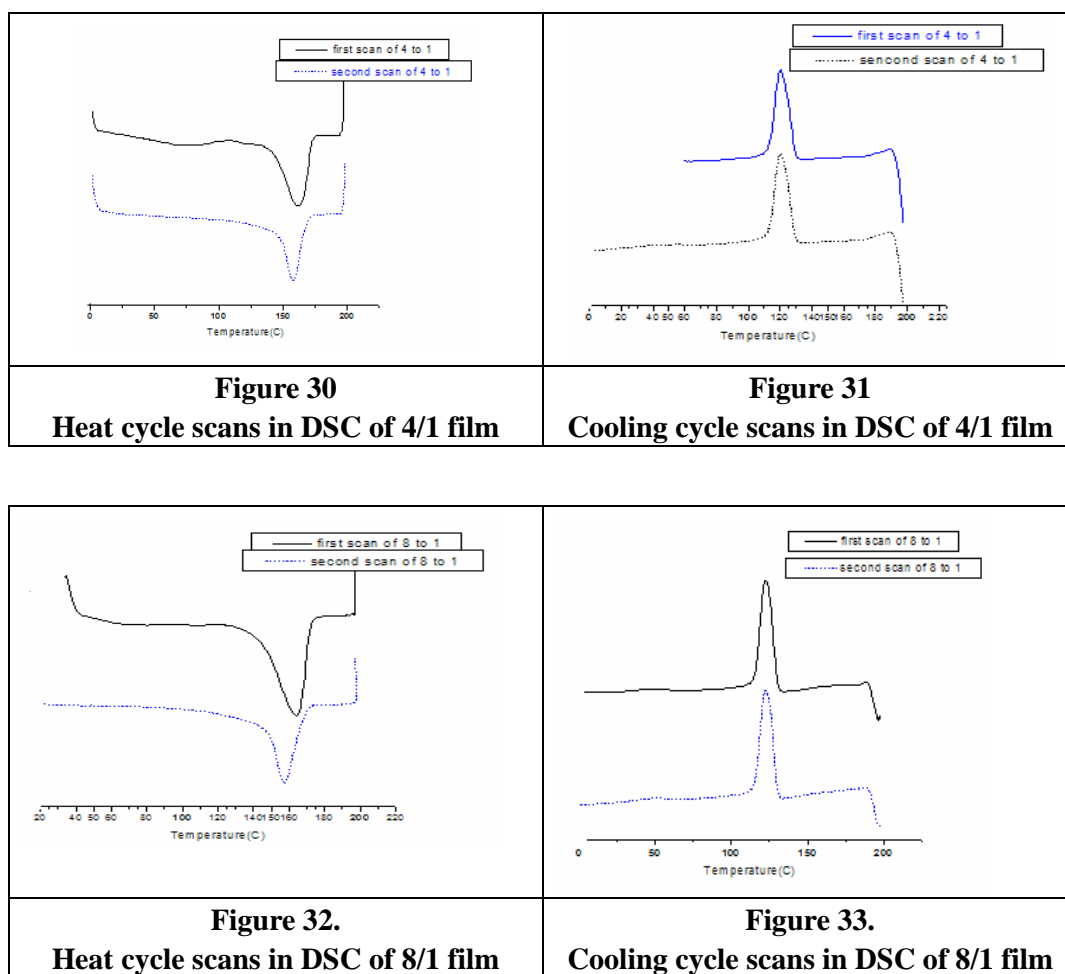


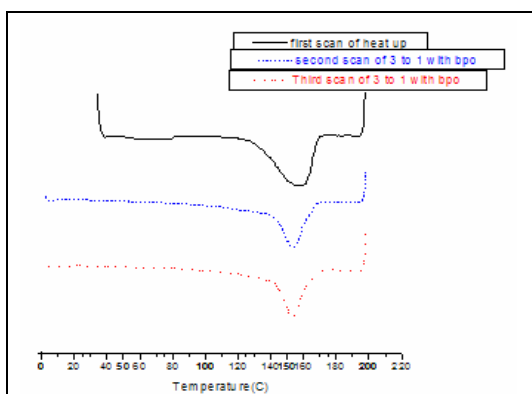


Figure 28 displays stack plots of the melting peaks from the first, second and third heating cycle scans for PVdF/poly[(4(5)-VIm/VIm<sup>+</sup>TFSI](3/1)<sub>V</sub>. The melting temperature of the first scan is slightly higher than that of the second scan, and the peak of the first scan is a broader. After the membrane had been heated to 200°C, the crystals that reformed were smaller, resulting in a lower melting point and narrower peak width. Figure 29 displays stack plots of the recrystallization peaks from the first, second and third cooling cycle scans for PVdF/poly[(4(5)-VIm/VIm<sup>+</sup>TFSI](3/1)<sub>V</sub>. No differences were observed between the first and second scan for the recrystallization peaks.

The characteristic features of heating and cooling scans in the DSC thermograms of the 4/1 and 8/1 composites were analogous to those described for the 3/1 composite. Figures 30–33 display DSC thermograms for the 4/1 and 8/1 composites.



DSC thermograms of composite films doped with 0.1% by weight of dibenzoylperoxide were similar to those of peroxide-free PVdF/poly[(4(5)-VIm/VIm<sup>+</sup> TFSI)] films. Figures 34-39 display the respective heating and cooling curves for the composites containing 0.1% by weight of dibenzoylperoxide.



**Figure 34.**  
Heat cycle scans in DSC of 3/1 film  
with dibenzoylperoxide

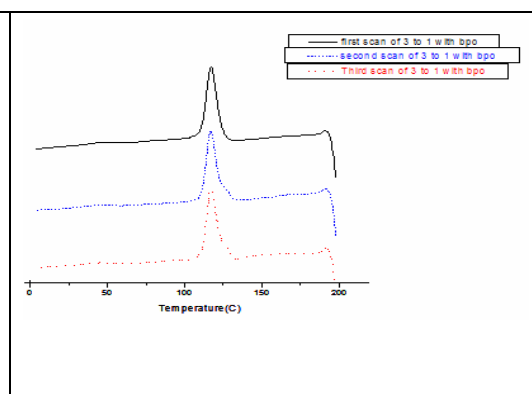


**Figure 35.**  
Cooling cycle scans in DSC of 3/1 film  
with dibenzoylperoxide

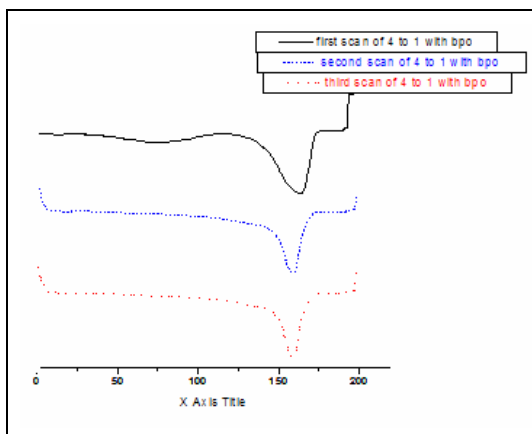


**Figure 36.**  
Heat cycle scans in DSC of 4/1 film with  
dibenzoylperoxide

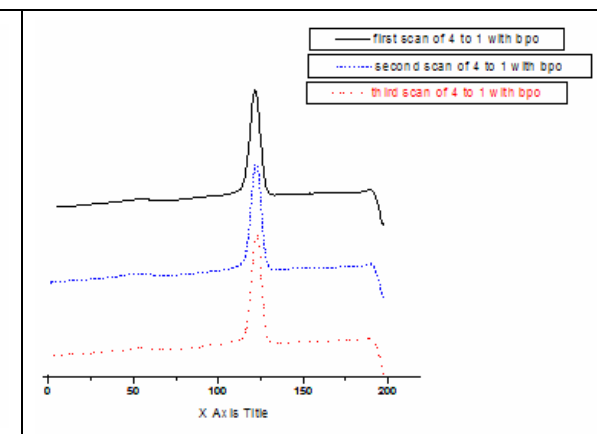
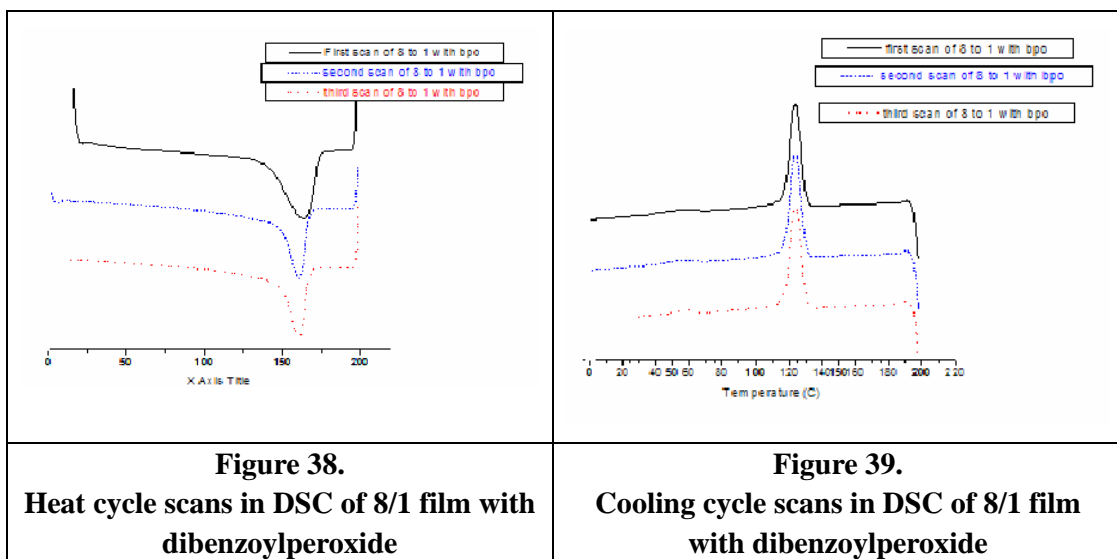


**Figure 37.**  
Cooling cycle scans in DSC of 4/1 film with  
dibenzoylperoxide



Crystallinity of these composites was tabulated and compared. The data is shown in Table 4.

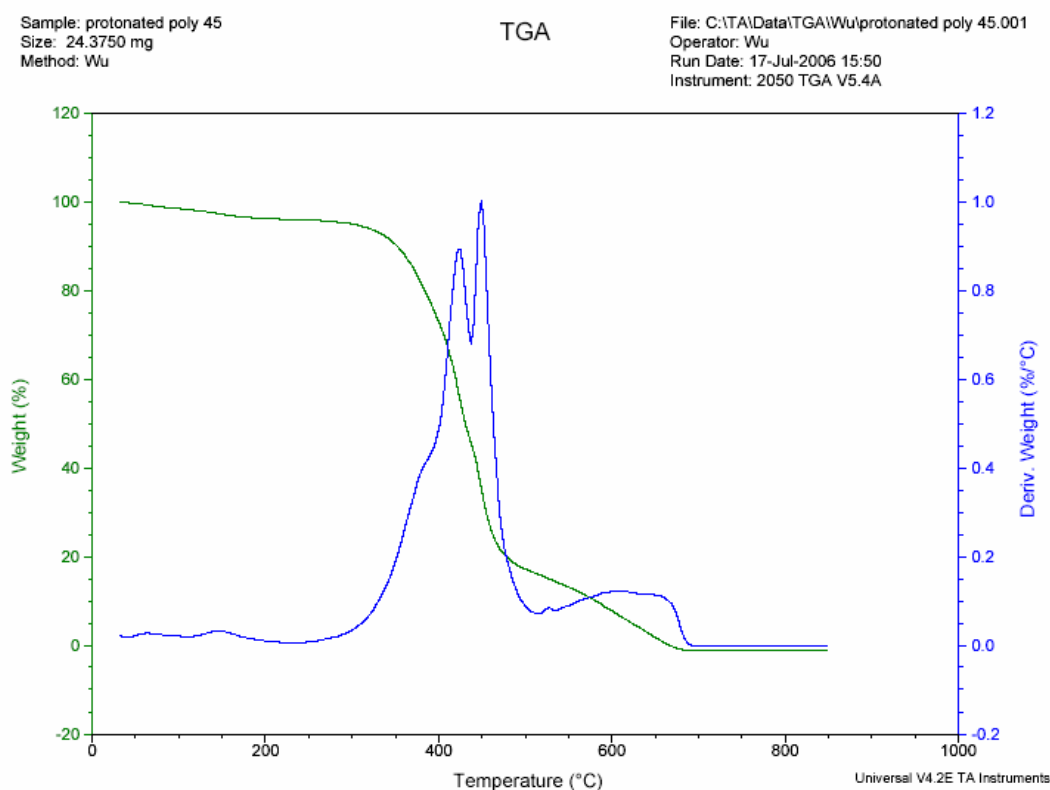
Polymer blends	Crystallization temperature(°C)	$\Delta H$ for 100% crystalline polymer( J/g)	Crystallinity (%)
3/1	121.63	21.59	20.60
3/1 with dibenzoylperoxide	125.42	24.63	23.50
4/1	120.27	24.68	23.55
4 to 1 with dibenzoylperoxide	122.77	25.25	24.09
8/1	122.74	28.25	26.96
8/1 with dibenzoylperoxide	123.95	37.64	35.92
PVdF	127.43	27.25	26.00

**Table 4. Crystallinity of the composite films.**

All recrystallization temperatures were measured at their corresponding peak values. The theoretical latent heat for 100% crystallinity of Kynar®301 is 104.8 J/g. From the Table 4, it appears that films doped with dibenzoyl peroxide have more crystallinity than films that did not contain peroxide. It may be that dibenzoyl peroxide is acting as a classic nucleating agent. One can also see that the 3/1 and 4/1 composites of PVdF/poly[(4(5)-VIm/VIm<sup>+</sup> TFSI)] have lower crystallinity than pure PVdF. Given that the crystalline component is PVdF, this is not a surprise.

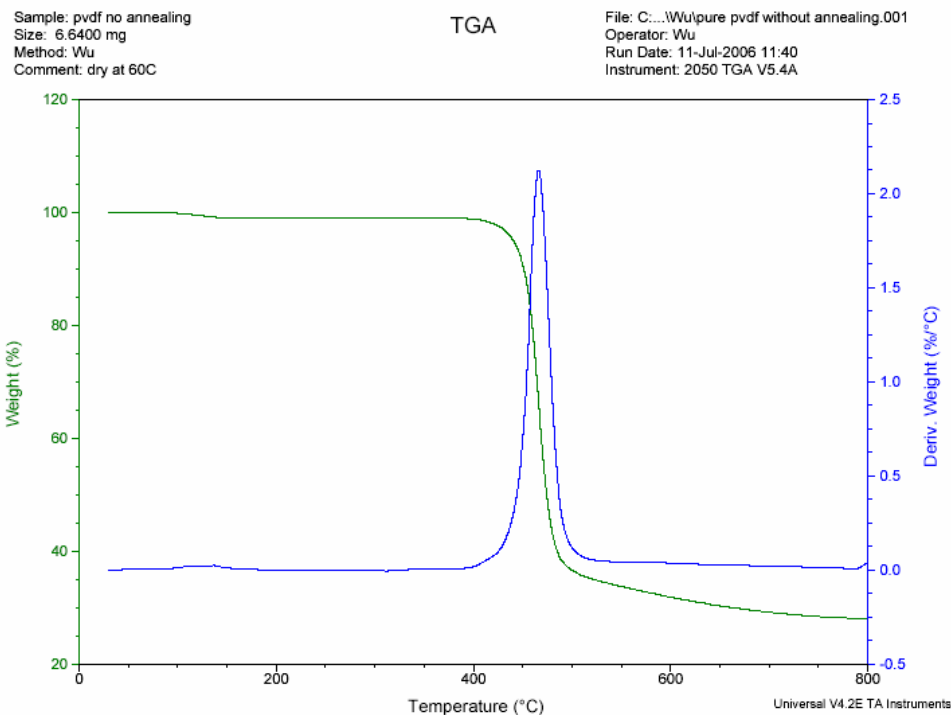
### 3. Thermal Gravimetric Analysis (TGA)

Thermal Gravimetric Analysis (TGA) was employed to examine the thermal stability of the composite films. As specified in the experimental section, a typical running process for TGA was to first heat to 800°C at a rate of 10°C/min and then to hold the temperature at 800°C for 2 minutes. Figure 40 shows the TGA spectrum for poly[(4(5)-VIm/VIm<sup>+</sup>TFSI)]. One can see that the protonated poly[4(5)vinylimidazole] starts to decompose at around 350°C and that there is a change in the slope around 450°C. Decomposition is complete at about 700°C with no residual mass.



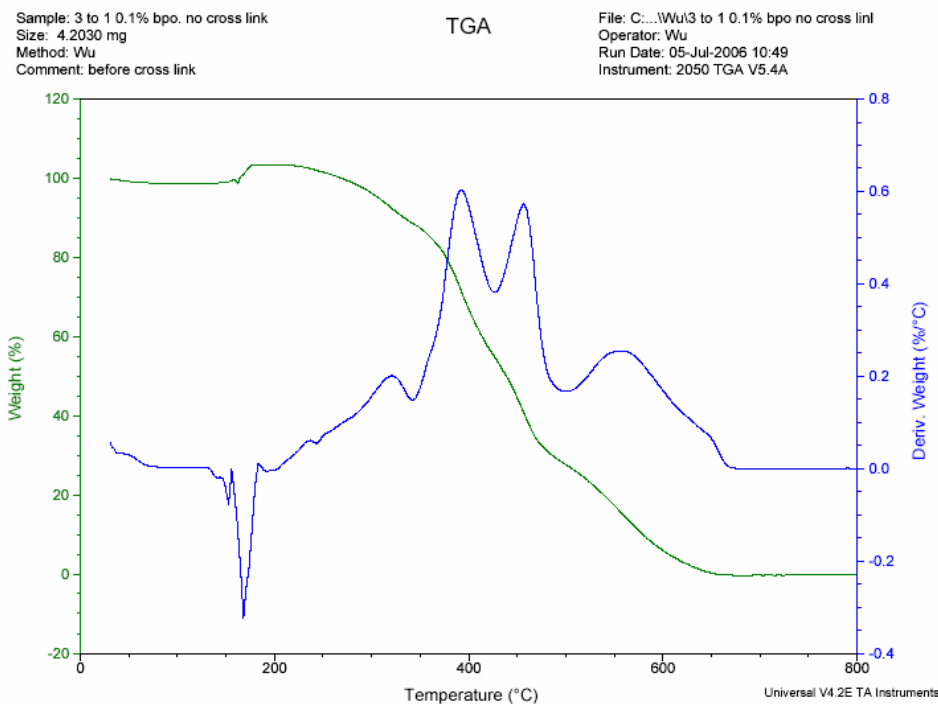
**Figure 40. TGA of Poly[(4(5)-VIm/VIm<sup>+</sup>TFSI)]**

Figure 41 shows the TGA spectra for pure PVdF. The material starts to decompose at around 400°C and asymptotes a residual mass of about 30% by weight at about 500°C.



**Figure 41. TGA of PVdF**

In Figure 42, the TGA spectrum for a film cast from the 3/1 PVdF/poly[(4(5)-VIm/VIm<sup>+</sup>TFSI)] solution with 0.1 % dibenzoylperoxide is shown. Decomposition starts at around 350°C. This is the same temperature at which the onset of decomposition was observed for poly[(4(5)-VIm/VIm<sup>+</sup>TFSI)] in Figure 40. There is an increase in the slope of the weight loss curve at about 400°C. This corresponds to the start of decomposition of PVdF. At about 500°C, the slope of the weight loss curve decreased and, when the heating cycle was stopped at 800°C there was no residual mass. The presence of poly[(4(5)-VIm/VIm<sup>+</sup>TFSI)] in the composition clearly promotes the complete thermal decomposition of PVdF.



**Figure 42. TGA of 3/1 PVdF/poly[(4(5)-VIm/VIm<sup>+</sup> TFSI]**

TGA scans of the 4/1 and 8/1 PVdF/poly[(4(5)-VIm/VIm<sup>+</sup> TFSI] composites, with and without 0.1% dibenzoylperoxide, were similar to those describe above for the 3/1 composite. Figure 43 shows the TGA scan of a film cast from a solution of the 4/1 PVdF/poly[(4(5)-VIm/VIm<sup>+</sup>TFSI] composite with 0.1% dibenzoyl peroxide that had not been annealed at 200°C prior to TGA analysis. One can clearly see weight loss in the temperature range between 80°C and 150°C. This is the temperature range in which dibenzoylperoxide is decomposed. The major cause of weight loss in this temperature range, however, is the evaporation of residual DMF form a film dried at ambient temperature.

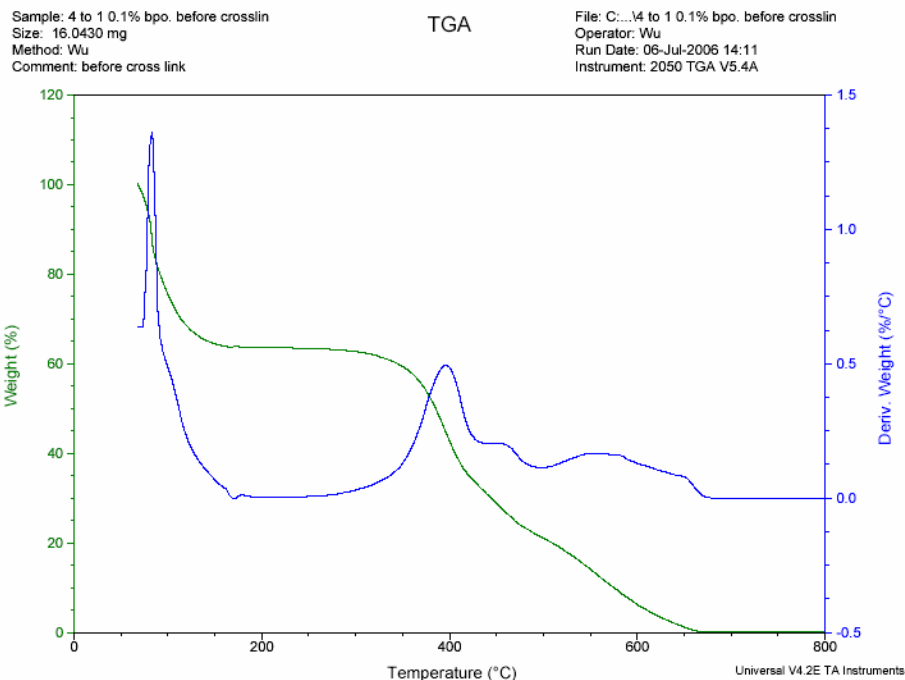


**Figure 43. TGA of 4 to 1 film before crosslinking with dibenzoyl peroxide**

The rest of the decomposition process is almost the same as was observed in Figure 44 which displays the TGA scan of a 4/1 PVdF/poly[(4(5)-VIm/VIm<sup>+</sup> TFSI] composite with 0.1% dibenzoyl peroxide was annealed at 200°C prior to TGA analysis.

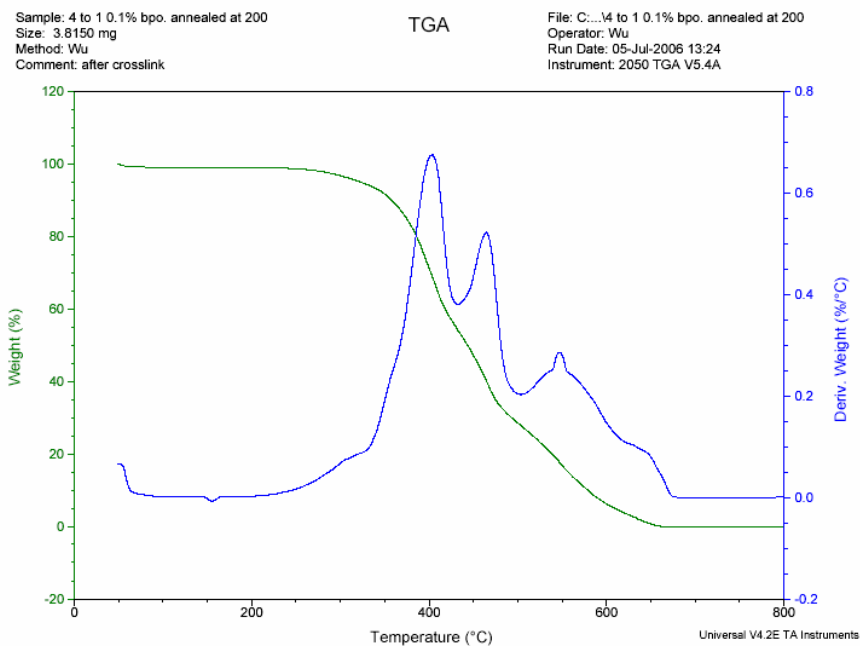


**Figure 44. TGA of 4 to 1 film after crosslinking with dibenzoyl peroxide**

Analogous TGA profiles were observed in the spectra of films cast from 8/1 solutions of PVdF/poly[(4(5)-VIm/VIm<sup>+</sup> TFSI] composite with 0.1% dibenzoyl peroxide which were dried at ambient temperature and which were annealed at 200°C. Figures 45 and 46 display TGA scans of the annealed and non-annealed films, respectively.

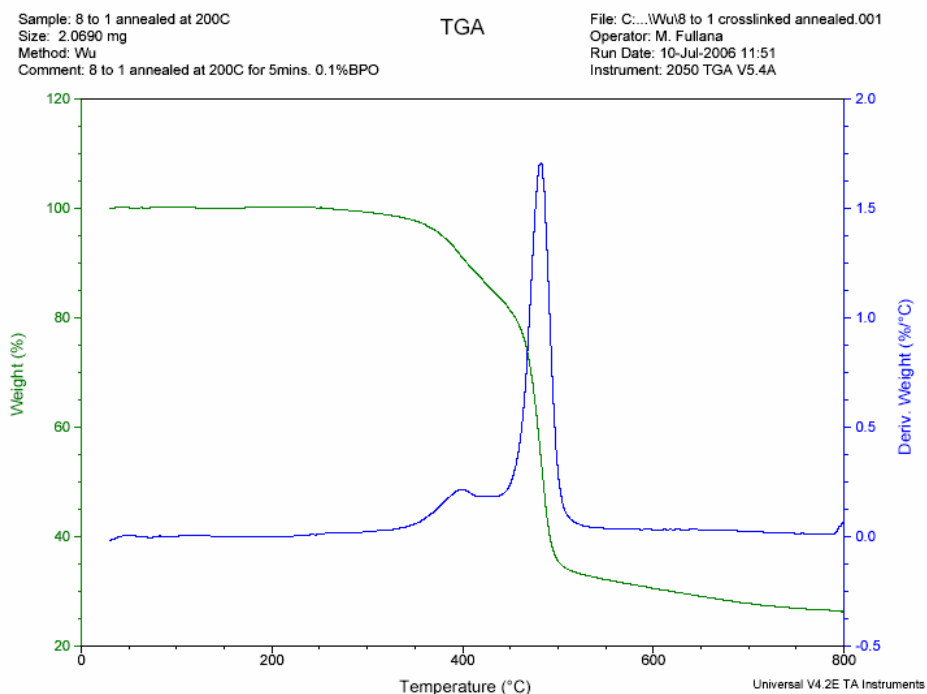


**Figure 45** TGA of 8 to 1 film after crosslinking with dibenzoyl peroxide



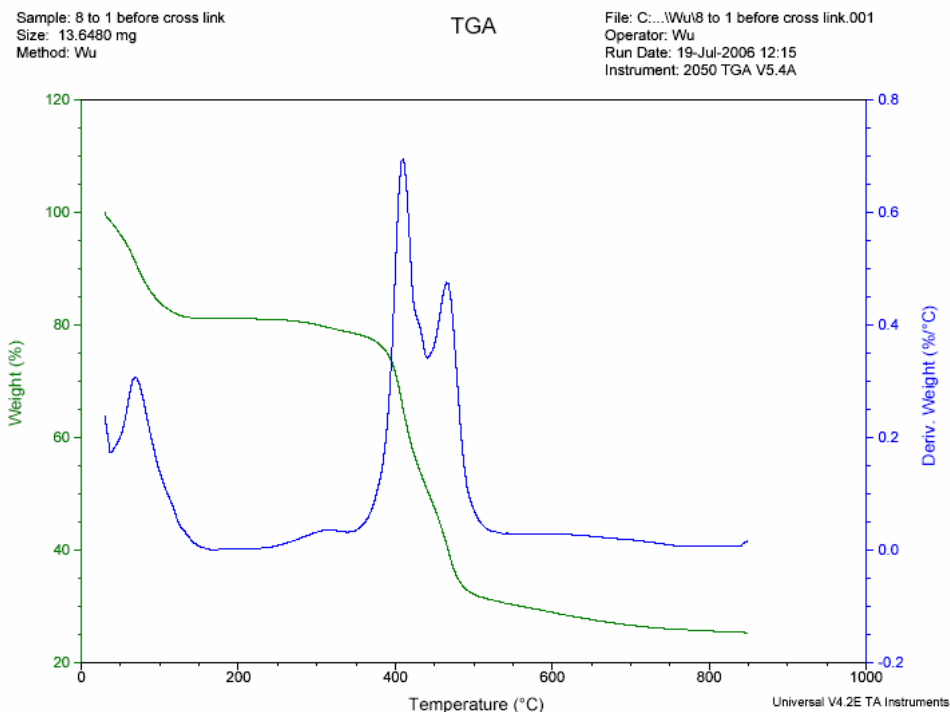


**Figure 46. TGA of 8/1 film before cross linking with dibenzoyl peroxide**

One should note that, as in the case of pure PVdF, residual mass remained after pyrolysis of the 8/1 composites. There was not a sufficient amount of poly[(4(5)-VIm/VIm<sup>+</sup>TFSI)] in the composite to promote complete decomposition.

### C. Proton conductivity

Proton conductivity of composite films was evaluated by Dr Timothy Fuller at GM Fuel Cell Activities in Honeoye Falls, NY. Three cross-linked composite films of PVdF/poly[(4(5)-VIm/VIm<sup>+</sup>TFSI)] after annealing at 200°C were evaluated. The conductivity was tested in a fuel cell at 80°C with varied relative humidity. The conductivity of Nafion®112 at 80° C as a function of % relative humidity was also measured as a comparison reference. A plot of the humidity dependence of the conductivity of Nafion®112 at 80° C is shown in Figure 47.

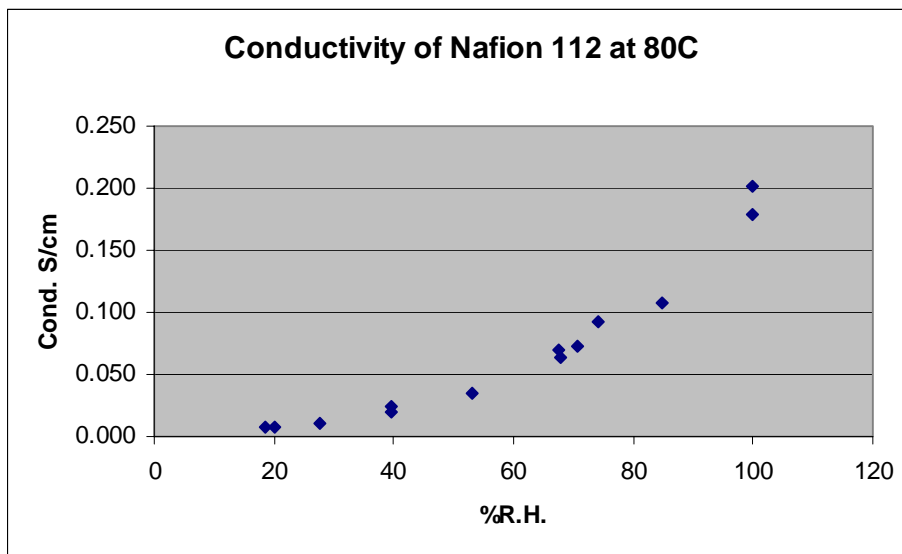


**Figure 47. Humidity dependence of conductivity of Nafion®112 at 80° C.**

The data clearly shows that the conductivity increases with the increase of relative humidity, reaching its highest point (0.18 S/cm) at 100 % relative.

A plot of the humidity dependence of the conductivity of the 3/1 PVdF/poly[(4(5)-VIm/VIm<sup>+</sup> TFSI] film at 80°C is shown in Figure 48.

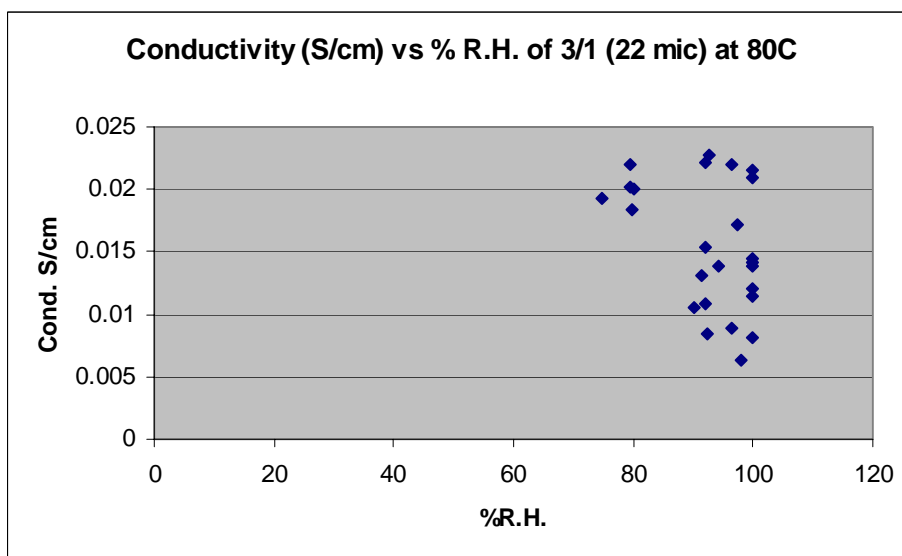


**Figure 48. Humidity dependence of conductivity of a 3/1 PVdF/poly[(4(5)-VIm/VIm<sup>+</sup> TFSI] composite film at 80°C.**

One can see that the 3/1 PVdF/poly[(4(5)-VIm/VIm<sup>+</sup> TFSI] composite film shows a high level of conductivity at 100% relative humidity with initial values greater than

0.02 S/cm. The conductivity only drops slightly at 80% RH.

The humidity dependence of the conductivity of the 4/1 PVdF/poly[(4(5)-VIm/VIm<sup>+</sup>TFSI)] composite film at 80°C is shown in Figure 49.

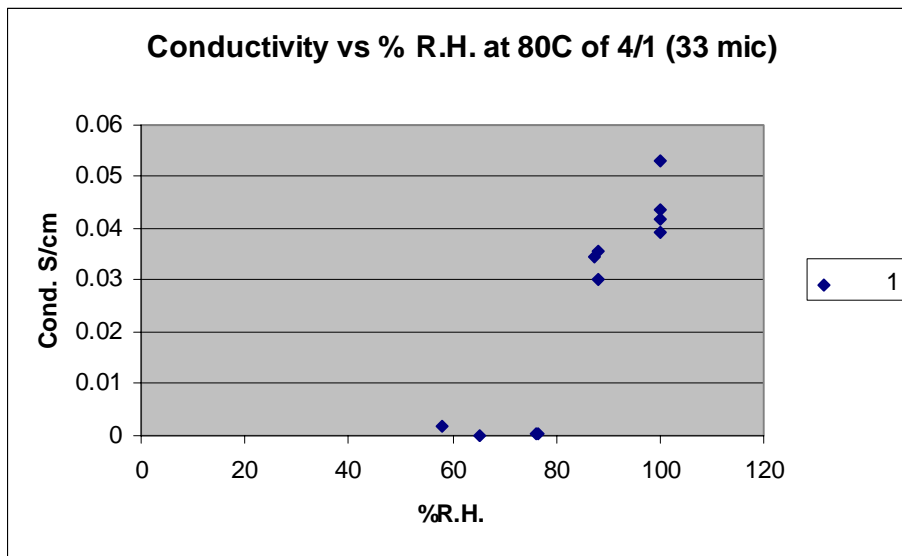


**Figure 49. Humidity dependence of conductivity of a 4/1 PVdF/poly[(4(5)-VIm/VIm<sup>+</sup> TFSI)] composite film at 80°C.**

The 4/1 PVdF/poly[(4(5)-VIm/VIm<sup>+</sup> TFSI)] composite film exhibited a similar humidity dependence of conductivity to that of the 3/1 PVdF/poly[(4(5)-VIm/VIm<sup>+</sup>TFSI)] composite film. Initial values of conductivity at 100% relative humidity were in excess of 0.05 S/cm.

The 8/1 PVdF/poly[(4(5)-VIm/VIm<sup>+</sup> TFSI)] composite film did not show any proton conductivity. At this low volume fraction of poly[(4(5)-VIm/VIm<sup>+</sup> TFSI)] there was not enough protonated poly[4(5)vinylimidazole] to form a continuous proton transport path.

The implications of these initial proton conductivity measurements are quite exciting. However, there are significant questions that must be addressed before this work can be published. The first issue that must be addressed is the apparent instability or scatter of the conductivity data over time. The reason for this may be associated with some leaching of the protonated poly (4(5)vinylimidazole) from the films during the test. While minimal loss of mass was measured in the water extraction experiments, those experiments were performed at ambient temperature. It will no doubt be

necessary to prepare composite systems from which protonated poly[4(5)vinylimidazole] cannot be leached, even at 100°C. In addition, proton conductivity measurements at low RH and at temperatures in excess of 100°C must be carried out. The thickness of the films employed in this initial round of experiments was ~25 microns. Proton conductivity must be evaluated in thicker films, films ranging in thickness from 50 microns to 150 microns.

The initial seemed to data say that the 4/1 PVdF/poly[(4(5)-VIm/VIm<sup>+</sup>TFSI)] composite film was more conductive than the 3/1 film. If this is indeed true, the reason would have to be related to differences in morphology whereby more contiguous through-film, poly[(4(5)-VIm/VIm<sup>+</sup>TFSI)] pathways are formed in the 4/1 composite than in the 3/1 composite.

### **Summary and Next Steps**

Composite proton exchange membranes were fabricated by casting films of poly[(4(5)-VIm/VIm<sup>+</sup>TFSI)] and PVdF, from mixed dimethylformamide (DMF) solutions. The phase, composition and morphology of these composites were examined by differential scanning calorimetry (DSC), and hot-stage polarized microscopy. Thermal stability was evaluated by thermal gravimetric analysis (TGA). Proton conductivity was in a fuel cell test fixture evaluated at GM Fuel Cell Activities in Honeoye Falls, NY.

DSC thermograms were characterized by a crystalline melt for the PVdF component at ~169°C. All composites displayed a well-form exothermic peak for recrystallization of PVdF at ~121°C. The melting and recrystallization characteristics of PVdF in the composites were substantially identical to those of pure PVdF. In its homogeneous state, poly[(4(5)-VIm/VIm<sup>+</sup>TFSI)] exhibited a glass transition temperature, T<sub>g-mid</sub>, of -30°C. Incorporation of benzoyl peroxide resulted in a slight increase in crystallinity of the 3/1 and 4/1 compositions and a substantial increase in crystallinity of the 8/1 composite. Crystallinity increased slightly as the volume fraction of PVdF was increased.

Classic crystalline spherulites were observed by polarized optical microscopy in

films cast from DMF and dried at temperatures below the melting point of PVdF. On heating to 200°C on the hot-stage microscope, crystals melted to reveal a rather amorphous dark field with thin worm-like inclusions which were presumed to arise from the poly[(4(5)-VIm/VIm<sup>+</sup>TFSI)] phase. On cooling to ambient temperature, the background field became progressively brighter, however, no structure that might be associated with the reformation of crystallites was observed. This was presumably a result of submicroscopic size of the crystallites.

TGA spectra of the all composite films were characterized by two transitions, one at 300°C corresponding to the decomposition of poly[(4(5)-VIm/VIm<sup>+</sup>TFSI)], and one at 450°C which corresponds to the decomposition of PVdF. Mass loss corresponded well with the mass fractions of the two components of the composite.

Proton conductivity was measured as a function of relative humidity at 80°C. Conductivity (0.05 S/cm) approaching that exhibited by Nafion® 112 (0.18 S/cm) was realized in the 4/1, PVdF/poly[(4(5)-VIm/VIm<sup>+</sup>TFSI)] composite film. Substantial conductivity (0.02 S/cm) was also measured in the 3/1 composite films. No measurable proton conductivity was observed in films of the 8/1 composite. We believe that this is the first instance in which such high proton conductivity levels have been realized in a polymer system where a Grotthuss mechanism of proton transport might be invoked. These results are very exciting and may point the way to the preparation of membranes exhibiting high levels of proton conductivity at elevated temperature and low relative humidity. Much work, however, remains to be done before composite membranes that might actually be used in vehicular systems can be realized.

Additional experiments that are outlooked include:

- preparation of PVdF composite films from which poly[(4(5)-VIm/VIm<sup>+</sup>TFSI)] cannot be leached,
- evaluation of proton conductivity at temperatures in excess of 100°C,
- visualization of the morphology and distribution of the poly[(4(5)-VIm/VIm<sup>+</sup>TFSI)] component of the composites,
- systematic variation of the level of prolongation with TFSI, and
- preparation of composites with various PVdF copolymers.

## References

- 1 [www.fueleconomy.gov/feg/fcv\\_PEM.html](http://www.fueleconomy.gov/feg/fcv_PEM.html)
- 2 [www.fuelcells.org/basics/types.html](http://www.fuelcells.org/basics/types.html)
- 3 Grot, W. *‘Chimie Ingenieur Technik* **1978**, 50(4), 299-301.
- 4 Ren, X.; Wilson, M.S.; Gottesfeld, S.; *J. Electrochem. Soc.*, **1996**, L12,143.
- 5 Steck, A.; in *Proceedings of the First International Symposium on New Materials for Fuel Cell Systems*, (Savadogo, O; Roberge, P.R; Veziroglu, T.N; eds.), Montreal, Canada, July 9-13, **1995**, p.74.
- 6 Antonucci, P.L.; Arico, A.S.; Creti, P.; Ramunni, E.; Antonucci, V; *Solid State Ionics*, **1999**, 125, 431.
- 7 Alberti, G.; Casciola, M.; *Annu. Rev. Mater. Res.* **2003**, m33, 129–54
- 8 Helmer-Metzmann, F.; Osan, F.; Schneller, A.; Ritter,H.; Ledjeff, K.; Nolte, R.; Thorwirth,R.; *U.S. Patent* 5,438,082 (**1995**).
- 9 Kerres, J.; Cui,W.; Eigenberger, G.; Bevers, D.; Schnurnberger, W.; Fischer, A.; Wendt, H.; in *Proceedings of the 11th Hydrogen Conference*, (Veziroglu,T.N.; Winter, C.J.; Baselt, J.P.; Kreysa, G.; eds.), Stuttgart, Germany, June 23-28, **1996**, p.1951.
- 10 Hogarth, M.; Glipa, X.; High Temperature Membranes for Solid Polymer Fuel Cells, *Johnson Matthey Technology Centre*, **2001**.
- 11 Nolte, R.; Ledjeff, K.; Bauer, M.; Mülhaupt, R.; *J. Membrane Sci.* **1993**,83, 211-220.
- 12 Kobayashi, T.; Rikukawa, M.; Sanui, K.; Ogata, N.; *Solid State Ionics*, **1998**, 106, 219
- 13 Yen, S-P.; Narayanan, G.; Halpert, E.; Graham, A.; Yavrouian; *U.S. Patent* 5,795,496 (**1998**).
- 14 Savinell, R.; Yeager, E.; Tryk, D.; Landau, U.; Wainright, J.; Weng, D.; Lux, K.; Litt, M.; Rogers, C.; *J. Electrochem. Soc.*, **1994**, L46,141
- 15 Wainright, J.S.; Wang, J.-T.; Weng, D.; Savinell, R.F.; Litt, M.; *J. Electrochem. Soc.*, **1995**, L121,142.
- 16 Buckley, A.; Stuetz, D.E.; Serad, G.A.; in *Encyclopedia of Polymer Science and Engineering*, (2nd ed., John Wiley & Sons, New York), **1988**, Vol. 11.
- 17 Watanabe,M.;Uchida,H.;Seki,Y.;Emori,M.;Stonehart, P.; *J.Electrochemical.Soc.* **1996**, 143, 3847.
- 18 Antonucci , P.L.; Arico , A.S.; Cretý , P.; Ramunni , E.; Antonucci, V.; *Solid State Ionics* **1999**,125, 431–437.
- 19 Kenneth A. Mauritz, *Materials Science and Engineering*, **1998**,C 6, 121-133.
- 20 Apichatachutapan, W.; Moore, R. B.; Mauritz, K. A. J.; *Appl. Polym. Sci.* **1996**, 62, 417.

- 
- 21 Shao, P. L.; Mauritz K. A.; Moore, R. B.; *Chem. Mater.* **1995**, 7, 192.
  - 22 Robertson M. A. F.; Mauritz, K. A.; *J. Polym. Sci.: B. Polym. Phys.* **1998**, 36, 595.
  - 23 Mauritz, K. A.; Payne, J. T.; *Journal of Membrane Science*, **2002**, 168 (1-2), pp. 39-51.
  - 24 Chang, H.; Kim, J.R.; Cho, J.H.; Kim, H.K.; Choi, K.H.; *Solid State Ionics*, **2002**, 14,8 601-606.
  - 25 Smith, T.W.; private communication "Options in Materials for Direct Methanol Fuel Cells", June 28, **2002**.
  - 26 Alberti G.; In *Membranes*, ed. Dept.Sci. Tech., **1992**, pp. 295–311. New Delhi: Oxford& IBH
  - 27 Peled, E.; Duvdevani, T.; Melman, A.; *Electrochem. Solid-State Lett.* **1998**, 1(5), 210.
  - 28 Peled, E.; Duvdevani, T.; Aharon, A.; Mellman, A.; *Electrochem. Solid-State Lett.* **2000**, 3 (12), 525.
  - 29 Susan, M.A.B.H.; Yoo, M.; Nakamoto, H.; Watanabe, M.; *Chem. Lett.*, **2003**, 32, 836.
  - 30 Münch, W.; Kreuer, K. D.; Silvestri, W.; Maier, J.; Seifert, G. *Solid State Ionics* **2001**, 145, 437
  - 31 Zhou, Z.; Liu, R.; Wang, J.; Li, S.; Liu, M.; Bre'das, J-L.; *Journal of Physical Chemistry*, **2005**, 127, 10824-10825.
  - 32 Li, S.; Zhou, Z; Zhang. Y.; Liu, M.; *Chem. Mater.*, **2005**, 17, 5884-5886.
  - 33 Densmore, C. G.; Rasmussen, P. G.; Goward, G. R.; *Macromolecules*, **2005**, 38, 416-421.
  - 34 Pu, H.; Meyer, W. H.; Wegner, G.; *Macromolecular Chemistry and Physics* **2001**, 202, 1478-1482.
  - 35 Bozkurt, A.; Meyer, W.H.; *Solid State Ionics*, **2001**, 138, 259-265.
  - 36 Susan, M.A.B.H.; Noda, A.; Mitsushima, S.; Watanabe, M.; *Chem. Commun.*, **2003**, 938.
  - 37 Fuller, J.; Breda, A.C.; Cartin, R.T.; J. *Electrochem. Soc.* **1997**, 144, L67
  - 38 Overberger, C. G.; Kawakami, Y.; *Journal of Polymer Science: Polymer Chemistry Edition*, **1978**, 16, 1237-1248.
  - 39 Kerres, J. A; *Journal of Membrane Science*, **2001**, 185, 3-27.
  - 40 Glipa, X.; Bonnet, B.; Mula, B.; Jones, D.J.; Rozière, J.; *J. Mater. Chem.* **1999**, 9, 3045
  - 41 <http://www.alhyde.com/alh028wp.html>